LMAL

TECHNICAL NOTES

NATIONAL ADVISORY COMMITTEE FOR AERONAUTICS

No. 354

AN INVESTIGATION OF THE PHENOMENON OF SEPARATION IN THE AIR FLOW AROUND SIMPLE QUADRIC CYLINDERS

By John F. Parsons and Jarvis A. Wallen

Washington
November, 1930

To be returned to
the files of the Langley
Memorial Aeronautical
Laboratory

NASA Technical Library
3 1176 01431 9496

NATIONAL ADVISORY COMMITTEE FOR AERONAUTICS.

TECHNICAL NOTE NO. 354.

AN INVESTIGATION OF THE PHENOMENON OF SEPARATION IN THE AIR FLOW AROUND SIMPLE QUADRIC CYLINDERS.*

By John F. Parsons and Jarvis A. Wallen.

Summary

The tests, conducted at the Guggenheim Aeronautic Laboratory of Stanford University, to investigate the phenomenon of separation in the air flow past geometric bodies are described in this report.

The experimental work consisted of wind-tunnel pressure-distribution tests and determinations of the line of separation on one circular and two elliptical cylinders. All three models had the same perimeter, and were mounted in the tunnel so as to give two-dimensional flow symmetrical about the major axis. The speeds of test employed were approximately 40, 57, 72, and 91 feet per second. Theoretical pressure-distributions for the models were computed for purposes of comparison.

The tests show a recession of the line of separation and an improvement of the agreement between the experimental and theoretical pressure-distributions with an increase in either fineness ratio or velocity. A given increment of velocity produces a constant recession of the line of separation regardless of fineness ratio. For each model, irrespective of scale, sep-

*Thesis submitted in partial fulfillment of the requirements for the degree of Engineer in Mechanical Engineering Aeronautics, Stanford University.

aration occurs after adverse pressures act through a constant distance. This distance, however, increases with fineness ratio.

The most important result of the investigation is the unique relation which was found to exist between the pressure at the point of separation and the minimum pressure. The ratio of these pressures, the pressures being reckoned from stagnation pressure as a datum, is shown to approximate 91% and is independent of change of scale or fineness ratio.

Introduction

An ideal fluid flowing past a disturbing body divides at the nose of the body, streams along the sides, with perfect slip, to the rear where it unites and continues downstream without turbulence or loss of energy to the system. Real fluid motion, however, separates from the after portion of the disturbing body where a wake is formed, and energy is expended in dragging this region along behind the body. This turbulent area originates in the boundary layer where, under the influence of an unknown sequence of events, the flow departs from the solid generating vortex sheets, which bound the "dead water" region. Where the wake is small, viscous forces outside the boundary layer are negligible (Reference 1) and are disregarded in the outer region in which the fluid, except for the presence of the wake, behaves essentially as an ideal fluid.

When the wake is large, as it often is in practice, a con-

siderable loss of energy, chargeable to form drag, occurs. The problem of reducing this loss is a difficult one and its solution is impeded by the present lack of knowledge concerning boundary-layer phenomena. The efficiency of an airfoil is still limited, because, at a certain critical attitude, for a given wing profile, separation occurs over the upper surface, which so hinders the circulation that the lift decreases and the form drag becomes large. It is known that form drag is proportional to the strength and breadth of the vortex street discharged from the surfaces of solid bodies (References 2 and 3), but these values cannot be predicted by theory and the problem of form drag remains unsolved.

At present, it is believed that a flow of a real fluid around a solid body without any wake or separation does not exist. The location of the line of separation and the width of wake are known to vary with Reynolds Number. It is also a current theory that separation occurs only in the presence of an adverse pressure gradient, and that it is preceded by marked thickening and retardation of the layer of fluid which is undergoing shear. Two types of boundary-layer flow appear possible, laminar or turbulent flow. It has recently been suggested (References 4 and 5) that transition from the laminar to the turbulent type is characterized by a rapid thickening of the layer. The thickness varies with $\sqrt{\nu x/V}$ for laminar flow over flat plates (Reference 6), and according to Von Karman, the thick-

ness for turbulent flow is proportional to $x^{0.8}$. If δ is the thickness of the boundary layer, transition from laminar to turbulent flow can be shown to occur when a critical value of Reynolds Number $V\delta/\nu$, is reached. (Reference 4).

If some reliable criteria were available for the prediction of the line of separation, a more intelligent attack upon the problem of boundary-layer control could be made. The known methods of control are: to accelerate the surface layer before it reaches the position at which separation normally occurs, and to delay separation by removing the stagnant fluid-layer as it forms. The latter method has had little practical application, while the former is used in wing slots, the N.A.C.A. type of engine cowling, etc. If efficient control of real fluid motion is to be attained, more information relative to boundary-layer phenomena is needed.

The purpose of this investigation was to study the influences of pressure and velocity distributions, and of Reynolds Number upon separation of the flow from the surfaces of solid bodies. Cylinders having quadric sections, to facilitate prediction of theoretical flow characteristics, were prepared for pressure-distribution testing and for determination of the line of separation. All the perimeters were made equal to afford a basis of comparison between models. It was hoped that correlation and analysis of the results might lead to the identification of conditions for separation.

Pages incorrectly numbered (5 not used) - no omission of text.

A 1
B 1.5-r
C 4-1

Models and Apparatus

The three cylinders which were tested have equal perimeters and fineness ratios of 1.0, 1.5, and 4.0. Their cross sections are: Model A, circular, 6" diameter; Model B, elliptical, major axis 7.128", and minor axis 4.752"; Model C, elliptical, with major and minor axes of 8.792" and 2.198", respectively. Each model consisted of an accurately-machined, brass center section, eight inches in length, extended beyond the limits of air stream by two laminated redwood end pieces, or dummies. An internal tension tierod running the entire length of the model stiffened it against air loads. Figures 1, 2, 3, and 4 are photographs of the cylinders.

Pressure leads of copper tubing, 0.052" outside diameter, were sweated into holes drilled in the center section (Figure 8), at the locations given in Table I; the tubes extend lengthwise through the model to a manometer. To align the model into the wind, two check pressure orifices were provided on opposite sides of the model, equidistant from the nose. The location of these orifices was determined by an inspection of the theoretical pressure-distribution curves for each model. They were intended to be placed where the pressure gradient was large.

The center section is accurate to 0.001" in the offsets. The end pieces were verified, by application of their construction templates, to 0.01"; however, a slight twist was present in the elliptical dummies at distances of 24" from the center section.

The models, set up for test, were placed in the tunnel to give two-dimensional flow symmetrical about the major axis.

The tests were conducted in an open circuit, free-jet type of wind tunnel, with a throat diameter of eight feet and a free-jet length of six feet.

A pressure operated regulator, which controlled the fan speed, limited the variation in air-stream velocity to ±0.5%.

The differential pressure balance (Fig. 5) measures the pressure reduction in the experiment chamber.

Pressure components normal to the surface of the center section were measured by a liquid-filled, multiple-tube manometer (Figs. 6 and 7). Tubes were left open at intervals along the manometer to determine a reference line of static pressure. Silhouette manometer records were obtained in a darkened room with photographic paper and an electric light (Fig. 9). The method was accurate in so far as the errors due to parallax and shrinkage were negligible.

Method of Test

The pressure reduction at a static pressure plate in the entrance cone, some distance upstream from the experiment section, is a measure of the dynamic pressure of the jet. The relationship is obtained by a survey of the free jet with an N.A.C.A. Pitot tube, and is constant regardless of the obstructions placed in the jet. For convenience in testing, it is

desirable to obtain the dynamic pressure of the jet q, by a measurement of the pressure reduction in the experiment chamber, or the room depression. The relation between q and the room depression is, however, modified by the introduction of obstructions in the jet. This modification necessitates a calibration of room depression in terms of the reduction of pressure at the static plate. Therefore, a separate calibration was made for each model.

Correct alignment was obtained by the rotation of the model about its longitudinal axis until the pressures were equal at the two orifices symmetrically located with respect to the model's nose. The alignment was checked for each test.

The discovery of an apparent scale effect upon the symmetry of flow about Model B was traced to small errors in orifice location and asymmetry of the wooden sections of the model. To obtain symmetric flow around the test section it was necessary to adjust the model to such a position that the pressures at the auxiliary orifice and a symmetric point on the opposite side (located between orifices) were equal. The pressure at the symmetric point was obtained by a graphical interpolation between observed pressures for adjacent orifices.

The asymmetry of the wooden sections of the model produced a change in the direction of the air stream which varied approximately 1.5° within the range of speeds covered by the tests. An auxiliary test demonstrated, in so far as the flow around the test section was concerned, that this asymmetry had no im-

portant influence upon anything but the effective air stream direction and that reliable results might be obtained by realigning the model for each speed. The test referred to consisted in attaching to the model, 2 feet aft of the nose, a 36" x $\frac{1}{4}$" x $\frac{1}{4}$" wooden strip, to observe the effect of contour irregularities upon the flow pattern. The result was the production of no visible effect upon the pressures at the test section until the tip of the strip came within $\frac{1}{2}$" of the row of pressure orifices.

Through an error in the design of Model C the check orifices were placed at a position corresponding to that on the other models. This location is not on a steep portion of the pressure curve; the sensitivity in alignment, therefore, is not comparable with that of the other models, hence the method previously used was not satisfactory. Final alignment of Model C consisted of the measurement of the nose pressure over a sufficient range of angular settings to define a maximum value. The model, when placed at the angular setting corresponding to the maximum value of the nose pressure, was in accurate alignment to $\pm 0.2^{\circ}$, an amount comparable to the degree of accuracy in the alignment of the preceding models. As in Model B, the asymmetry of the wood sections of the model produced a change in air-stream direction necessitating alignment for each speed.

Each pressure-distribution test consisted in the making of a manometer record, and the recording of data necessary for ve-

locity determination. Two tests were made at each speed.

The line of separation was determined at velocities corresponding to those at which pressure-distribution tests were taken. The method used was to discharge hydrogen sulphide gas, from the pressure orifices, over a freshly painted band of white lead on the surface of the center section. The gas was supplied to individual orifices at a pressure practically equal to the surface pressure, thereby eliminating any violent ejection of the gas. The trend of the boundary-layer flow was established by the appearance of a brown stain formed when the gas reacted with the white lead. In these tests the farthest forward evidence of reverse flow indicated the line of separation; the turbulent effect on the after portion of the model was neglected.

Results

The results of the velocity calibrations appear in Table II and are self-explanatory.

Results of the pressure-distribution tests are tabulated in Tables III, IV, and V, and are presented in graphical form in Figures 10-21 inclusive. Pressures are expressed in the form P/P_n, the ratio of the pressure at any point on the perimeter to the nose pressure, and are independent of velocity. The positions of the orifices are defined in terms of the peripheral distance from the nose, in inches.

The results and explanation of the symbolic tabulation

of the tests to determine the line of separation are found in Table VI, and are graphically represented in Figure 22. General diffusion of the gas without definite direction of staining, when preceded by rearward flow and followed by forward flow, is taken as an indication of separation.

The theoretical pressure-distributions, for the models tested, were determined analytically (Reference 7), as shown in Table VII, and are plotted in Figures 23, 24, and 25.

Discussion

The theoretical and experimental pressure-distribution curves of Model A are grouped for comparison as shown in Figure 26. Similar graphs for Models B and C are shown in Figures 27 and 28.

A quantitative analysis of these pressure distributions will not be attempted because, in the method of test employed, only pressure components normal to the surface are measured and because, it is not known whether this pressure is generated solely by flow in the outer region, or whether it is due to the combined effects of outer fluid motion and boundary-layer flow. Qualitative conclusions of some merit, however, may be drawn from a study of the test results.

By comparing the curves of Figures 26, 27, and 28 either as distinct families or as corresponding curves of each group, it can be seen that the influence of change in shape is important.

As the fineness ratio, i.e., the ratio of maximum length to maximum width of section, increases, a retrograde movement of the line of separation occurs, so that, for any velocity over the range investigated, a given increment of fineness ratio produces a constant shift in the position of the line of separation; the curves of Figure 22 are, therefore, parallel. For a given fineness ratio, a study of the results shows that the distance between the point of minimum pressure and the line of separation is constant regardless of speed, and that this distance increases with an increase in fineness ratio (Table VIII). Evidence of pressure-drag reduction is found in the fact that the discrepancy between theoretical and experimental pressure-distribution decreases with an increase in fineness ratio.

From a consideration of any one of the three groups of curves (Figs. 26, 27, and 28) it is evident that the effects of change in scale are analogous to those produced by alteration of shape. As the scale of test increases, the line of separation recedes and the pressure drag is reduced. The approach of the experimental to the ideal pressure distribution with an increase in scale is more rapid and more consistent for Model A than for other models. The tests of Models B and C agree more nearly with the results predicted by theory. This is due to the fact that in the cases of Models B and C, the critical velocity has been greatly exceeded so that the boundary layer becomes turbulent before separation and, consequently, separa-

tion is delayed. In the case of Model A, the boundary layer is laminar up to the separation point at the lowest speed, and at other speeds the flow is in the transition stage.

A relation, independent of either change of scale or fineness ratio, was found to exist between the pressure at the point of separation and the minimum pressure. The pressures were reckoned from stagnation pressure. The value of this ratio is approximately 91% as determined in Table VIII. If the measured pressures indicate kinetic energy, then separation occurs after approximately 9% of the maximum kinetic energy available in the test has been returned to the system as potential or pressure energy.

A comparison of tests on Model A with the cylinder tests described in Reference 5, shows good agreement, as to scale effect, even though different tunnels and test methods were used. The present tests, however, fail to consistently check the conclusion drawn in Reference 5, that the marked inflection in the pressure-distribution curve indicates the region of separation.

Conclusion

The conclusions drawn from this work may be summarized as follows:

1. The effect of an increase in either fineness ratio or velocity, or both, on the air flow around a simple, quadric cylinder is a recession of the line of separation.

2. An improvement in agreement between the experimental and theoretical pressure distributions, resulting in the reduction of pressure drag, accompanies an increase in either fineness ratio or scale of test.

3. For any given increment of velocity, there is a constant recession of the line of separation regardless of the fineness ratio.

4. The peripheral distance between the point of minimum pressure and the line of separation remains constant for each model throughout the range of Reynolds Number investigated. An increase in fineness ratio increases this distance.

5. The ratio between the pressure at the line of separation and the minimum pressure, the pressures being reckoned from stagnation pressure, remains a constant value of approximately 91% for all the models, regardless of the velocity. Hence, if pressure reduction indicates conversion of potential energy into kinetic energy, then separation occurs after approximately 9% of the maximum kinetic energy of the particle has been returned to the system as pressure energy.

In the course of this investigation many interesting problems inviting further study presented themselves. A summary of these might be of aid for future investigators, and a few are outlined briefly as follows:

1. A determination of the effect of initial turbulence upon the boundary-layer flow.

2. A study of the effect of yaw and change of perimeter upon the results obtained in this investigation.

3. The prediction of the point of separation through some method other than that of experimentally derived pressure maps.

References

1. Prandtl, L. : Applications of Modern Hydrodynamics to Aeronautics. N.A.C.A. Technical Report No. 116, 1921.

2. Glauert, H. : Aerofoil and Airscrew Theory, 1926.

3. Karman, Th. V. : "Über den Mechanismus des Widerstandes den ein bewegter Körper in Flussigkeit, erfahrt," Göttingen Nachrichten, 1911.

4. Burgers, J. M. and van der Hegge Zijnen, B. G. : "Laboratorium voor Aerodynamica en Hydrodynamica der Technische Hoogeschool te Delft." Mededeeling, Nos. 5 and 6.

5. Fage, A. : The Airflow around a Circular Cylinder in the Region where the Boundary Layer Separates from the Surface. British A.R.C. Reports and Memoranda No. 1179, August, 1928.

6. Blasius, H. : "Grenzschichten in Flussigkeiten mit kleiner Reibung." Zeitschrift f. Math. u. Phys., 1908.

7. Zahm, A. F. : Flow and Drag Formulas for Simple Quadrics. N.A.C.A. Technical Report No. 253, 1927.

8. Defoe, George L. : Resistance of Streamline Wires, 1928.

TABLE I

ORIFICE PERIPHERAL DISTANCES FROM NOSE

Orifice	Model A in.	Model B in.	Model C in.
1	0.00	-0.03	0.00
2	0.26	+0.22	0.28
3	0.53	0.48	0.53
4	0.79	0.76	0.80
5	1.05	1.01	1.04
6	1.58	1.55	1.57
7	2.10	2.07	2.10
8	2.63	2.34	2.63
9	3.15	2.60	3.14
10	3.42	2.87	3.41
11	3.68	3.13	3.66
12	3.83	3.40	3.94
13	3.99	3.66	4.20
14	4.14	3.92	4.48
15	4.30	4.18	4.74
16	4.46	4.46	4.88
17	4.62	4.70	5.02
18	4.77	4.82	5.18
19	4.93	4.97	5.33
20	5.09	5.12	5.49
21	5.25	5.27	5.65
22	5.51	5.43	5.78
23	5.77	5.58	5.94
24	6.03	5.75	6.09
25	6.29	5.90	6.27
26	6.55	6.07	6.42
27	6.82	6.23	6.59
28	7.35	6.39	6.73
29	7.87	6.54	6.89
30	8.39	6.71	7.06
31	8.91	6.86	7.23
32	9.43	7.01	7.38
33	----	7.19	7.54
34	----	7.33	7.70
35	----	7.59	7.85
36	----	7.84	8.12
37	----	8.11	8.37
38	----	8.36	8.62
39	----	8.63	8.90
40	----	8.88	9.16
41	----	9.43	9.43

TABLE II

Velocity Calibration

q = dynamic pressure in lb./sq.ft.
R.D. = reduction in pressure in experiment chamber, lb./sq.ft.
P_s = static pressure in entrance cone, lb./sq.ft.

Free jet	q/R.D.	P_s/R.D.
On jet axis	0.8666	0.8008
24" above jet axis	0.8599	0.7976
24" below " "	0.8198	0.7980
24" right of jet axis	0.8704	0.8009
24" left of jet axis	0.8679	0.7965
Average	0.8569	0.7988

$$q = \frac{1}{2} \rho V^2 = \frac{1}{2} \frac{\Delta}{g} = 0.8569 \text{ R.D.}$$

$$V = \sqrt{2 \times 32.2 \times 0.8569 \frac{\text{R.D.}}{\Delta}}$$

$$= 7.43 \sqrt{\frac{\text{R.D.}}{\Delta}}$$

Model A:

P_s lb./sq.ft.	R.D. lb./sq.ft.	P_s/R.D.
0.57	0.75	0.7600
0.91	1.20	0.7580
1.48	1.93	0.7664
2.11	2.77	0.7618
2.99	3.87	0.7722
3.93	5.15	0.7632
5.95	7.74	0.7685
7.04	9.20	0.7656
8.50	11.05	0.7690
Average		0.7650

Free jet: P_s/R.D. = 0.7988
Model A : P_s/R.D. = 0.7650

$$\frac{q}{\text{R.D.}_{\text{model}}} = \frac{\dfrac{P_s}{\text{R.D.}_{\text{model}}}}{\dfrac{P_s}{\text{R.D.}_{\text{free jet}}}} \times \frac{q}{\text{R.D.}_{\text{free jet}}}$$

TABLE II (Cont.)

Velocity Calibration

$$V = 7.43 \sqrt{\frac{0.7650}{0.7988} \times \frac{R.D.}{\Delta}} = 7.27 \sqrt{\frac{R.D.}{\Delta}}$$

Model B:

P_s lb./sq.ft.	R.D. lb./sq.ft.	P_s/R.D.
0.67	0.87	0.7700
1.01	1.32	0.7652
2.23	2.86	0.7796
2.95	3.79	0.7782
3.31	4.26	0.7768
5.45	6.95	0.7840
6.83	8.70	0.7852
10.40	13.23	0.7860
Average		0.7781

$$V = 7.43 \sqrt{\frac{0.7781}{0.7988} \times \frac{R.D.}{\Delta}} = 7.34 \sqrt{\frac{R.D.}{\Delta}}$$

Model C:

P_s lb./sq.ft.	P_s/R.D.	R.D. lb./sq.ft.	P_s/R.D.
1.75	.778	2.25	0.7780
2.67	.790	3.38	0.7902
3.25	.784	4.15	0.7831
5.08	.800	6.35	0.8801
6.76	.791	8.55	0.7907
10.10	.788	12.83	0.7872
Average	.7851		0.7882
	.7885		

$$V = 7.43 \sqrt{\frac{0.7882}{0.7988} \times \frac{R.D.}{\Delta}} = 7.38 \sqrt{\frac{R.D.}{\Delta}}$$

TABLE III

Pressure Distribution - Model A

R.D. lb./sq.ft.	2.23	4.45	6.95	11.35
q lb./sq.ft.	1.83	3.65	5.70	9.31
Velocity ft./sec.	40.30	56.94	71.12	91.04

Orifice	P/P_n							
	A-1	A-1CH	A-2	A-2CH	A-3	A-3CH	A-4	A-4CH
1	1.00	1.00	1.00	1.00	1.00	1.00	1.00	1.00
2	1.00	1.00	0.97	0.97	0.97	0.96	0.97	0.97
3	0.86	0.88	0.87	0.87	0.88	0.86	0.87	0.87
5	0.60	0.60	0.57	0.60	0.57	0.57	0.55	0.54
7	-0.26	-0.26	-0.43	-0.44	-0.48	-0.51	-0.53	-0.56
8	0.71	0.71	1.00	1.01	1.10	1.11	1.16	1.20
9	1.03	1.03	1.49	1.49	1.62	1.65	1.72	1.78
10	1.03	1.03	1.61	1.62	1.81	1.85	1.88	1.97
11	0.97	1.00	1.68	1.69	1.92	1.95	2.05	2.13
12	1.00	1.00	1.78	1.78	2.05	2.07	2.19	2.28
13	0.97	0.91	1.76	1.76	2.09	2.12	2.26	2.35
15	0.88	0.86	1.64	1.65	2.06	2.09	2.28	2.38
16	0.88	0.86	1.60	1.60	2.03	2.04	2.27	2.38
17	0.88	0.86	1.56	1.57	1.94	1.96	2.25	2.34
18	0.91	0.88	1.54	1.56	1.88	1.90	2.13	2.24
19	0.86	0.83	1.49	1.50	1.82	1.82	2.08	2.20
20	0.88	0.86	1.46	1.46	1.80	1.80	2.02	2.12
21	0.83	0.77	1.32	1.31	1.71	1.73	1.96	2.03
22	0.83	0.80	1.15	1.15	1.38	1.37	1.76	1.90
23	0.86	0.83	0.99	0.99	0.87	0.87	1.16	1.29
24	0.77	0.74	0.85	0.83	0.56	0.60	0.76	0.86
25	0.77	0.71	0.82	0.79	0.48	0.49	0.49	0.56
26	0.77	0.77	0.76	0.75	0.43	0.45	0.39	0.43
27	0.77	0.77	0.74	0.75	0.41	0.43	0.35	0.40
28	0.77	0.74	0.71	0.71	0.39	0.42	0.33	0.36
29	0.77	0.74	0.71	0.71	0.41	0.42	0.34	0.36
30	0.77	0.77	0.71	0.69	0.39	0.42	0.34	0.36
31	0.71	0.71	0.65	0.64	0.41	0.40	0.33	0.36
32	0.74	0.74	0.67	0.65	0.41	0.41	0.33	0.36

TABLE IV

Pressure Distribution - Model B

R.D. lb./sq.ft.	2.13	4.52	7.08	11.33
q lb./sq.ft.	1.78	3.77	5.91	9.46
Velocity ft./sec.	39.27	57.14	71.63	90.89

Orifice	P/P_n							
	B-1	B-1CH	B-2	B-2CH	B-3	B-3CH	B-4	B-4CH
1	+1.00	+1.00	+1.00	+1.00	+1.00	+1.00	+1.00	+1.00
2	+ .97	+ .91	+ .94	+ .94	+ .94	+ .95	+ .95	.94
3	+ .75	+ .72	+ .74	+ .74	+ .75	+ .76	+ .76	.75
4	+ .44	+ .44	+ .45	+ .44	+ .47	+ .47	+ .47	.47
5	+ .12	+ .06	+ .16	+ .16	+ .17	+ .19	+ .18	.18
6	- .50	- .56	- .44	- .45	- .43	- .41	- .41	.40
7	- .91	- .97	- .89	- .90	- .88	- .86	- .87	.85
8	-1.12	-1.12	-1.07	-1.08	-1.07	-1.05	-1.05	1.04
9	-1.25	-1.28	-1.22	-1.23	-1.22	-1.20	-1.20	1.18
10	-1.34	-1.31	-1.34	-1.34	-1.34	-1.32	-1.32	1.30
11	-1.37	-1.41	-1.41	-1.42	-1.43	-1.39	-1.41	1.39
12	-1.47	-1.53	-1.52	-1.53	-1.54	-1.52	-1.51	1.48
13	-1.50	-1.53	-1.56	-1.57	-1.58	-1.56	-1.55	1.53
14	-1.53	-1.53	-1.60	-1.62	-1.63	-1.61	-1.59	1.57
15	-1.50	-1.50	-1.60	-1.62	-1.63	-1.63	-1.61	1.58
16	-1.37	-1.41	-1.62	-1.63	-1.66	-1.64	-1.63	1.61
17	-1.37	-1.31	-1.56	-1.56	-1.62	-1.59	-1.58	1.57
18	-1.41	-1.41	-1.57	-1.59	-1.63	-1.63	-1.60	1.58
19	-1.25	-1.28	-1.55	-1.56	-1.62	-1.59	-1.57	1.56
20	-1.25	-1.28	-1.54	-1.55	-1.61	-1.59	-1.57	1.55
21	-1.19	-1.22	-1.44	-1.47	-1.54	-1.52	-1.52	1.50
22	-1.25	-1.25	-1.44	-1.45	-1.53	-1.52	-1.51	1.49
23	-1.25	-1.25	-1.41	-1.44	-1.51	-1.49	-1.48	1.47
24	-1.19	-1.25	-1.39	-1.40	-1.46	-1.45	-1.43	1.42
25	-1.15	-1.16	-1.36	-1.37	-1.42	-1.41	-1.40	1.38
26	-1.06	-1.06	-1.36	-1.37	-1.41	-1.39	-1.37	1.35
27	-1.00	- .97	-1.34	-1.37	-1.39	-1.37	-1.33	1.31
28	- .84	- .84	-1.29	-1.30	-1.34	-1.33	-1.24	1.22
29	- .78	- .75	-1.09	-1.11	-1.20	-1.19	-1.07	1.05
30	- .72	- .69	- .78	-0.79	-0.97	-0.97	- .89	.88
31	- .62	- .62	- .63	- .64	- .80	- .80	- .79	.76
32	- .62	- .62	- .51	- .51	- .65	- .65	- .67	.65
33	- .62	- .62	- .38	- .38	- .52	- .51	- .52	.52
34	- .61	- .59	- .33	- .33	- .40	- .39	- .41	.40
35	- .56	- .56	- .23	- .23	- .25	- .25	- .25	.25
36	- .56	- .56	- .19	- .19	- .18	- .18	- .19	.19
37	- .50	- .50	- .15	- .15	- .14	- .14	- .15	.15
38	- .50	- .50	- .14	- .14	- .14	- .14	- .16	.15
39	- .50	- .50	- .14	- .14	- .14	- .14	- .17	.16
40	- .50	- .50	- .14	- .14	- .14	- .14	- .18	.17
41	- .47	- .47	- .12	- .12	- .12	- .11	- .14	.13

TABLE V

Pressure Distribution Tests - Model C

R.D. lb./sq.ft.	2.24	4.45	7.15	11.25
q lb./sq.ft.	1.89	3.75	6.04	9.52
Velocity ft./sec.	40.70	57.56	73.00	91.60

Orifice	P/P_n							
	C - 1	C-1CH	C - 2	C-2CH	C - 3	C-3CH	C - 4	C-4CH
1	+1.00	+1.00	+1.00	+1.00	+1.00	+1.00	+1.00	+1.00
2	.45	.45	.36	.36	.34	.34	.33	.33
3	.03	.05	- .03	- .03	- .04	- .05	- .05	- .05
4	- .18	- .18	.23	.23	- .24	.24	.24	.24
5	.24	.24	.29	.29	.31	.31	.30	.30
6	.34	.34	.39	.39	.41	.41	.40	.40
7	.42	.42	.45	.45	.47	.47	.46	.46
8	.42	.42	.47	.47	.49	.49	.47	.47
9	.42	.39	.47	.47	.48	.49	.48	.47
10	.42	.42	.48	.49	.50	.50	.49	.49
12	.45	.45	.51	.51	.52	.52	.50	.50
13	.45	.45	.51	.51	.53	.53	.52	.52
14	.47	.45	.51	.52	.54	.54	.52	.52
16	.42	.42	.49	.51	.51	.50	.50	.49
17	.42	.42	.49	.51	.51	.51	.50	.49
18	.42	.42	.49	.51	.52	.53	.52	.51
19	.42	.39	.48	.49	.50	.50	.50	.49
20	.45	.45	.51	.52	.52	.51	.50	.49
23	.45	.45	.51	.51	.51	.51	.49	.49
24	.45	.39	.49	.49	.51	.50	.49	.49
25	.39	.39	.48	.48	.50	.49	.49	.48
26	.39	.39	.47	.47	.50	.49	.48	.48
27	.39	.39	.45	.47	.47	.47	.46	.45
29	.37	.34	.45	.44	.48	.47	.46	.45
30	.39	.39	.45	.47	.47	.46	.44	.44
31	.34	.32	.41	.41	.44	.43	.42	.41
32	.34	.34	.41	.41	.43	.42	.39	.39
33	.34	.34	.40	.40	.40	.39	.37	.37
34	.39	.39	.40	.40	.41	.39	.35	.36
35	.37	.34	.36	.36	.37	.36	.32	.32
36	.34	.32	.31	.31	.27	.25	.20	.20
37	.24	.24	.21	.20	.13	.12	.06	.06
38	.08	.08	.05	.05	+ .03	+ .05	+ .08	+ .08
39	.11	.11	.00	.00	.10	.10	.14	.14
40	.11	.11	+ .01	+ .01	.08	.10	.13	.13
41	.05	.05	+ .05	.05	.11	.12	.14	.14

TABLE VI

Determination of the Line of Separation

Observations of Flow Direction

Model A:

Orifice	A - 1	A - 2	A - 3	A - 4
10	Rear.	Rear.	-	-
11	"	"	-	-
12	"	"	-	-
13	T.R.	"	-	-
14	T.	"	-	-
15	T.F.	"	Rear.	Rear.
16	"	T.R.	"	"
17	"	"	"	"
18	"	T.	T.R.	"
19	-	T.F.	T	T.R.
20	-	"	T.F.	"
21	-	"	"	T.
22	-	"	"	T.F.
23	-	-	"	"
24	-	-	"	"

Model B:

Orifice	B - 1	B - 2	B - 3	B - 4
16	Rear.	Rear	-	-
17	"	"	-	-
18	T.R.	"	-	-
19	T	"	-	-
20	T.F.	"	-	-
21	"	"	Rear.	Rear.
22	"	T.R.	"	"
23	"	"	"	"
24	-	T.	T.R.	"
25	-	T.F.	"	T.R.
26	-	"	T.F.	T.
27	-	"	"	T.F.
28	-	"	"	"
29	-	-	"	"

TABLE VI (Cont.)

Determination of the Line of Separation
Observations of Flow Direction

Model C:

Orifice	C - 1	C - 2	C - 3	C - 4
26	Rear.	-	-	-
27	T.R.	-	-	-
28	"	Rear.	-	-
29	"	"	-	-
30	T.	"	Rear.	-
31	T.F.	T.R.	"	-
32	"	"	T.R.	Rear.
33	"	T.	"	"
34	-	T.F.	T.	T.R.
35	-	"	T.F.	T.F.
36	-	"	"	"
37	-	-	"	"

Rear. = rearward flow.
T.R. = turbulent flow, rearward trend.
T. = turbulent flow, no dominant trend.
T.F. = turbulent flow, forward trend.

Location of Line of Separation

Test	Orifice No.	S	Velocity l/sec.
A-1	14	4.14	40.30
A-2	18	4.77	56.94
A-3	19	4.93	71.12
A-4	21	5.25	91.04
B-1	19	4.97	39.27
B-2	24	5.75	57.14
B-3	25-26	5.98	71.63
B-4	26	6.07	90.89
C-1	30	7.06	40.70
C-2	33	7.54	57.56
C-3	34	7.70	73.00
C-4	34-35	7.77	91.60

S = peripheral distance from nose in inches.

TABLE VII

Theoretical Pressure Distribution

Model A:

Diameter = 6"

$P/P_n = 1 - 4 \sin^2\theta$

θ = polar angle, polar coordinates.
S = peripheral distance from nose in inches.

S	θ	P/P_n
0.000, 9.425	0°, 180°	+1.0000
0.524, 8.901	10°, 170°	0.8794
1.047, 8.378	20°, 160°	0.5321
1.571, 7.854	30°, 150°	0.0000
2.094, 7.331	40°, 140°	-0.6427
2.618, 6.807	50°, 130°	-1.3473
3.142, 6.283	60°, 120°	-2.0000
3.666, 5.759	70°, 110°	-2.5321
4.190, 5.235	80°, 100°	-2.8794
4.712	90°	-3.0000

Model B:

$$P/P_n = 1 - \frac{(a + b)^2 y^2}{b^4 + c^2 y^2}$$

$a = \frac{\text{Major Axis}}{2} = 3.564''$ $\qquad (a + b)^2 = \frac{\quad}{5.940^2} = 35.284''^2$

$b = \frac{\text{Minor Axis}}{2} = 2.376''$ $\qquad b^4 = 31.870''^4$

$c^2 = (a^2 - b^2) = 7.057''^2$

$$P/P_n = 1 - \frac{35.284\ y^2}{31.870 + 7.057\ y^2}$$

y = ordinate in inches, of ellipse, major axis coincident with yy

S = peripheral distance from nose in inches

TABLE VII (Cont.)

Theoretical Pressure Distribution

Model B:

S	y	P/P_n
0.000, 9.425	0.000	+1.0000
0.202, 9.223	0.200	+0.9561
0.405, 9.020	0.400	+0.8289
0.608, 8.817	0.600	+0.6309
0.829, 8.596	0.800	+0.3794
1.065, 8.360	1.000	+0.0936
1.320, 8.105	1.200	-0.2088
1.598, 7.827	1.400	-0.5132
1.915, 7.510	1.600	-0.8088
2.284, 7.141	1.800	-1.0886
2.735, 6.690	2.000	-1.3484
3.347, 6.078	2.200	-1.5865
4.712	2.376	-1.7778

Model C:

$$P/P_n = 1 - \frac{(a + b)^2 \; y^2}{b^4 + c^2 \; y^2}$$

$$a = 4.396''; \; (a + b)^2 = \frac{\quad}{5.495^2} = 30.195''^2$$

$$b = 1.099''; \; b^4 = 1.459''^4$$

$$c^2 = a^2 - b^2 = 18.117''^2$$

y = ordinate, in inches, of ellipse, major axis coincident with yy

S = peripheral distance from nose in inches.

S	y	P/P_n
0.000, 9.425	0.000	+1.0000
0.101, 9.324	0.100	+0.8159
0.216, 9.209	0.200	+0.4468
0.351, 9.074	0.300	+0.1203
0.522, 8.903	0.400	-0.1087
0.727, 8.698	0.500	-0.2607
0.981, 8.444	0.600	-0.3620
1.293, 8.132	0.700	-0.4314
1.684, 7.741	0.800	-0.4804
2.191, 7.234	0.900	-0.5160
2.893, 6.532	1.000	-0.5425
4.715	1.099	-0.5624

TABLE VIII

Test	q lb./sq.ft.	a lb./sq.ft.	b lb./sq.ft.	a/b	c in.	d in.	c-d in.
A 1	1.83	3.44	3.74	0.921	4.14	3.27	0.87
2	3.65	9.30	10.01	0.921	4.77	3.90	0.87
3.	5.70	16.10	17.80	0.905	4.93	4.05	0.88
4	9.31	27.90	31.20	0.895	5.25	4.35	0.90
			average	0.910	average		0.88
B 1	1.78	4.03	4.51	0.897	4.97	3.68	1.29
2	3.77	9.00	9.85	0.914	5.75	4.25	1.50
3	5.91	14.20	15.68	0.907	5.98	4.48	1.50
4	9.46	22.30	24.70	0.904	6.07	4.53	1.54
			average	0.906	average		1.46
C 1	1.89	2.55	2.76	0.925	7.06	4.20	2.86
2	3.75	5.05	5.70	0.887	7.54	4.55	2.99
3	6.04	8.50	9.25	0.919	7.70	4.73	2.97
4	9.52	12.70	14.48	0.878	7.77	4.78	2.99
			average	0.902	average		2.95

NOTE:

a = pressure reckoned from a line of constant pressure = q at separation.
b = pressure reckoned from same reference line as a, at max. suction.
c = peripheral distance of line of separation from nose in inches..
d = peripheral distance of max. suction from nose in inches.

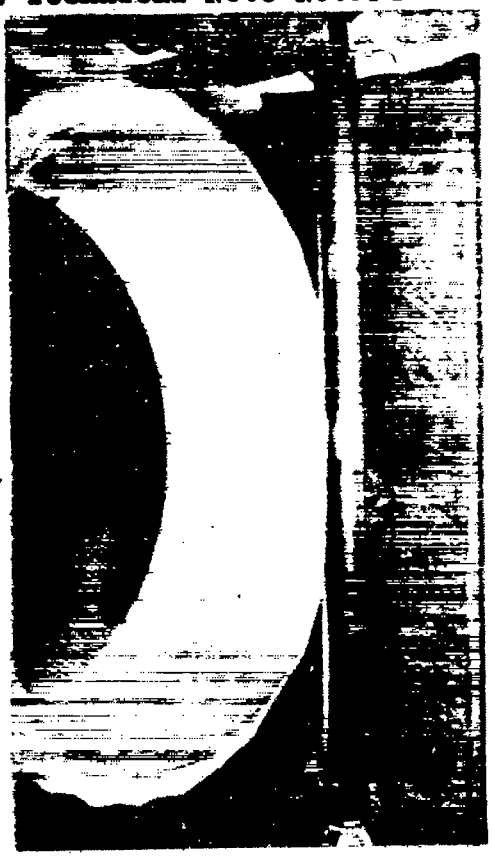

Fig.1

Model A

Fig.2

Model B

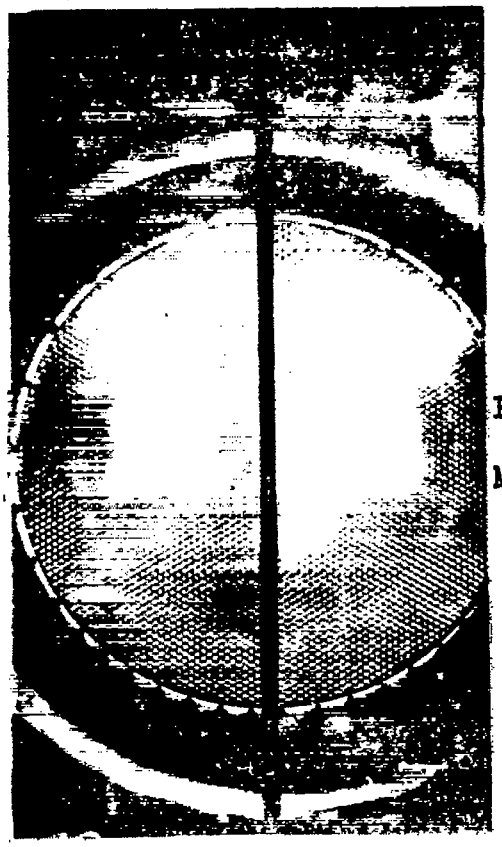

Fig.3

Model C

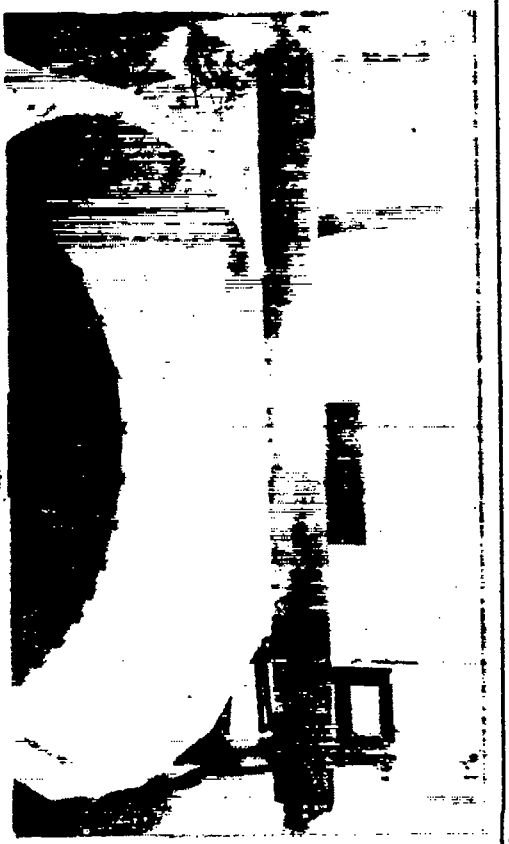

Fig.4

Model C

Fig.5

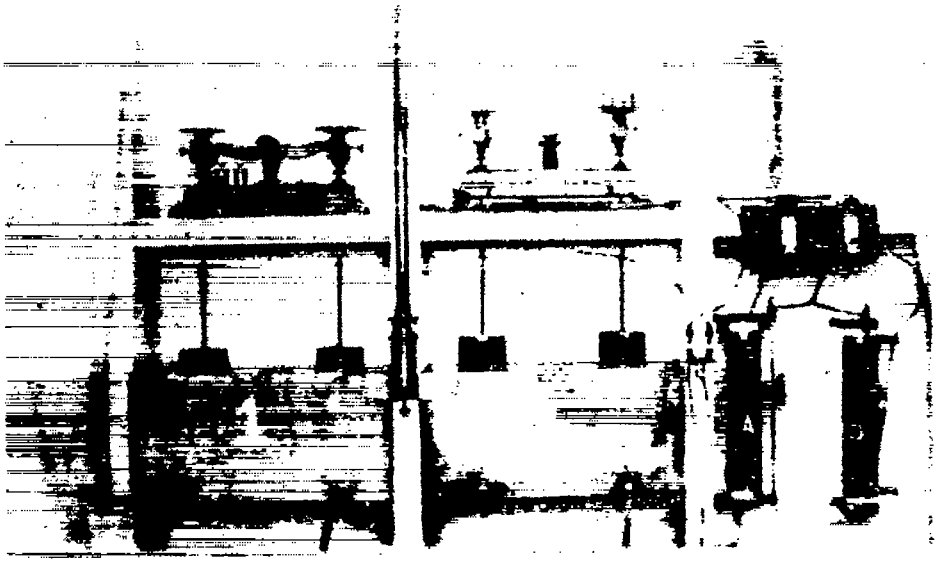

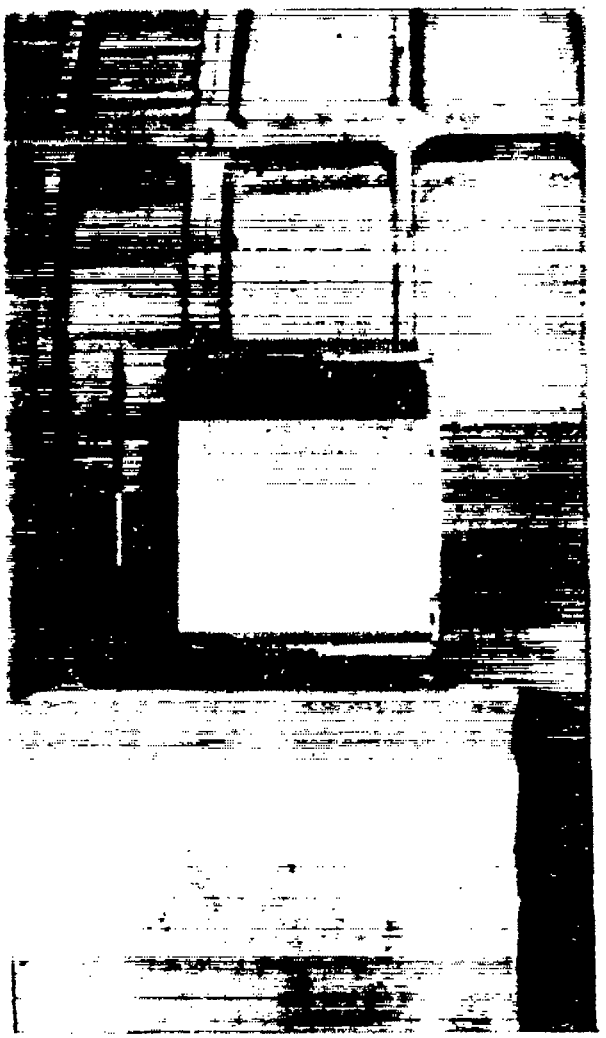

Fig.6

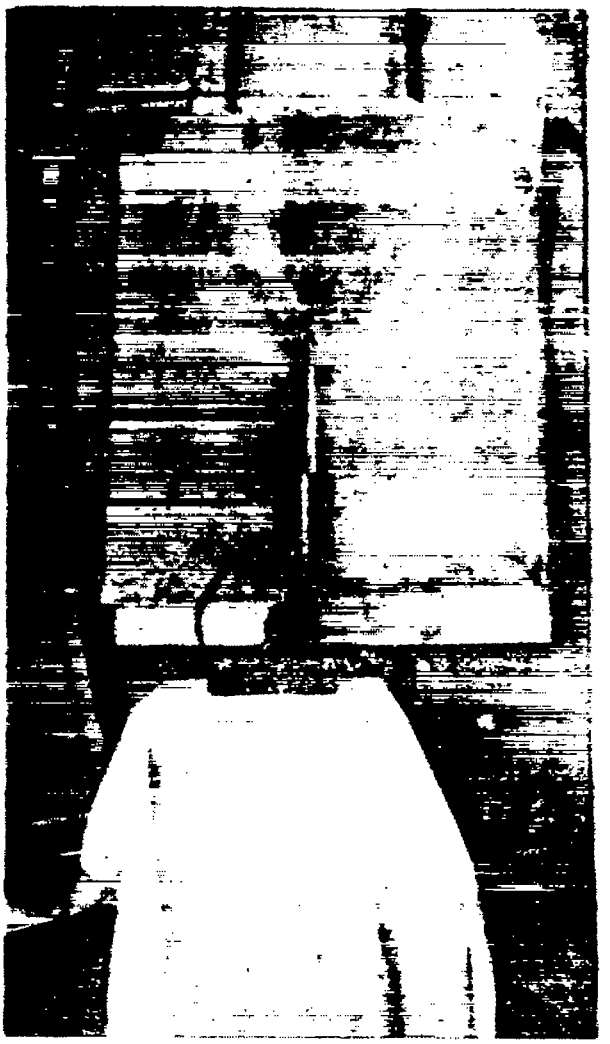

Fig.7

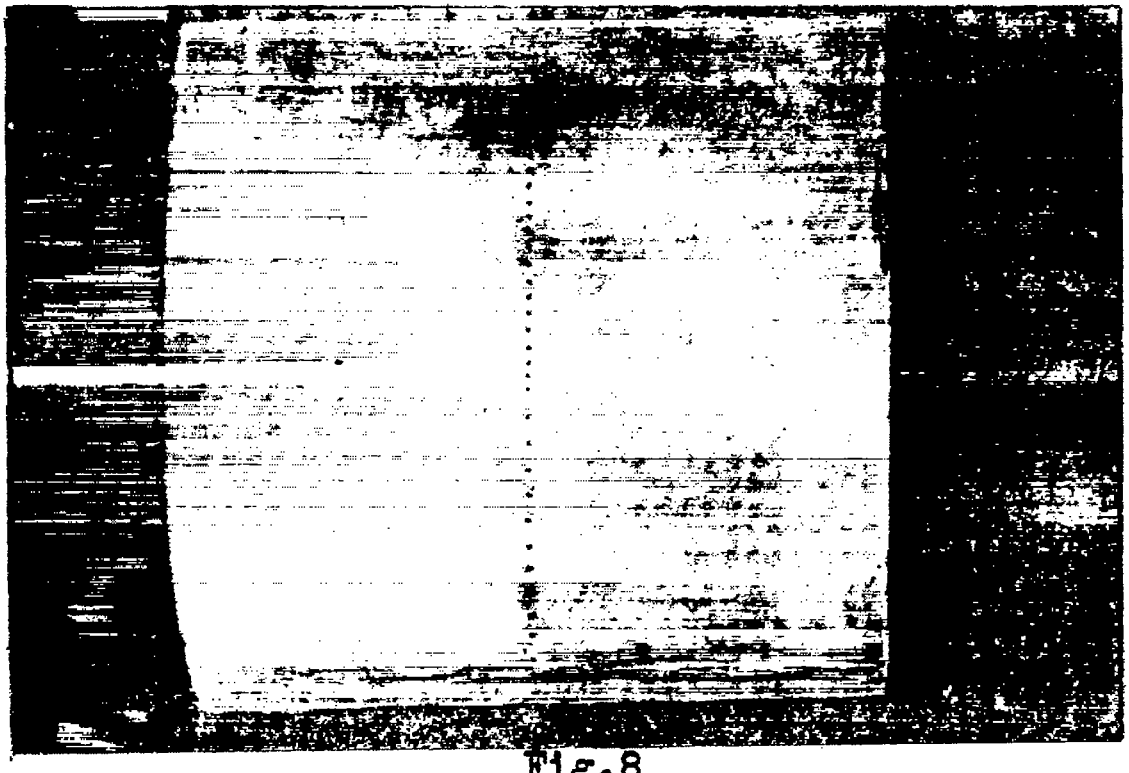

Fig.8

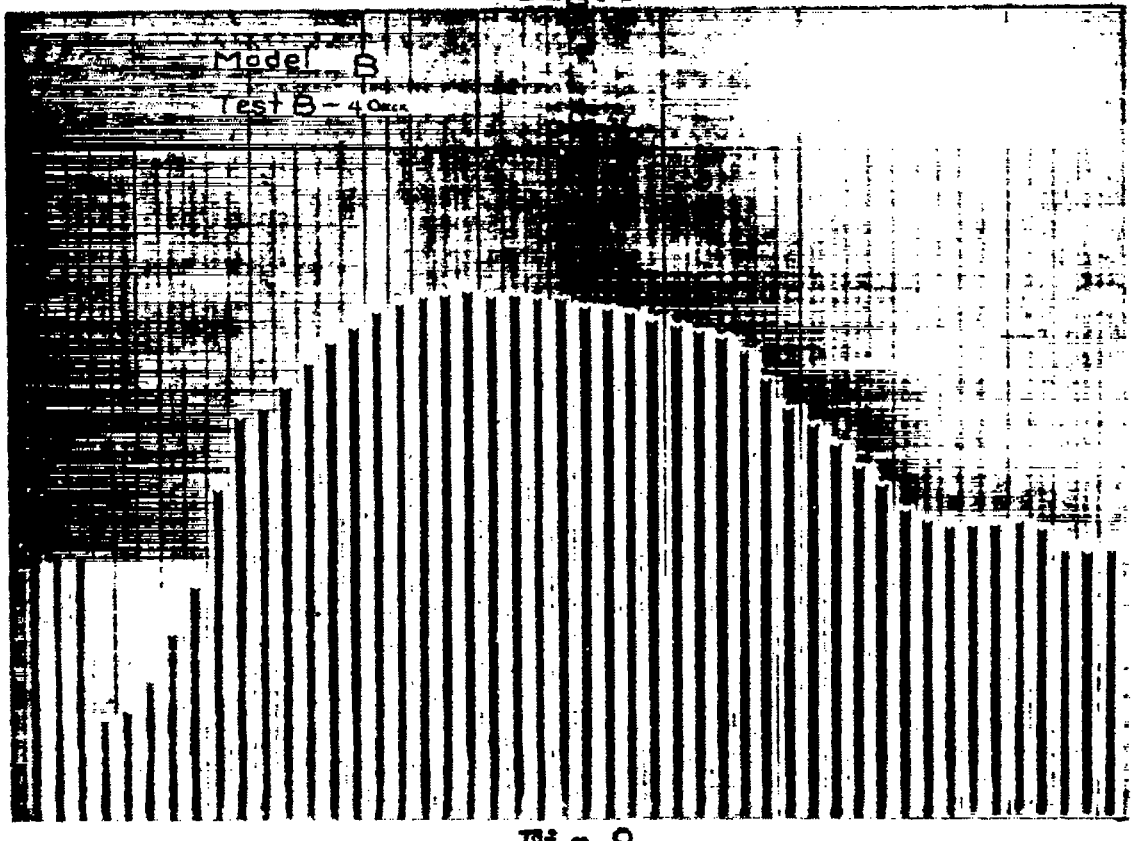

Fig.9

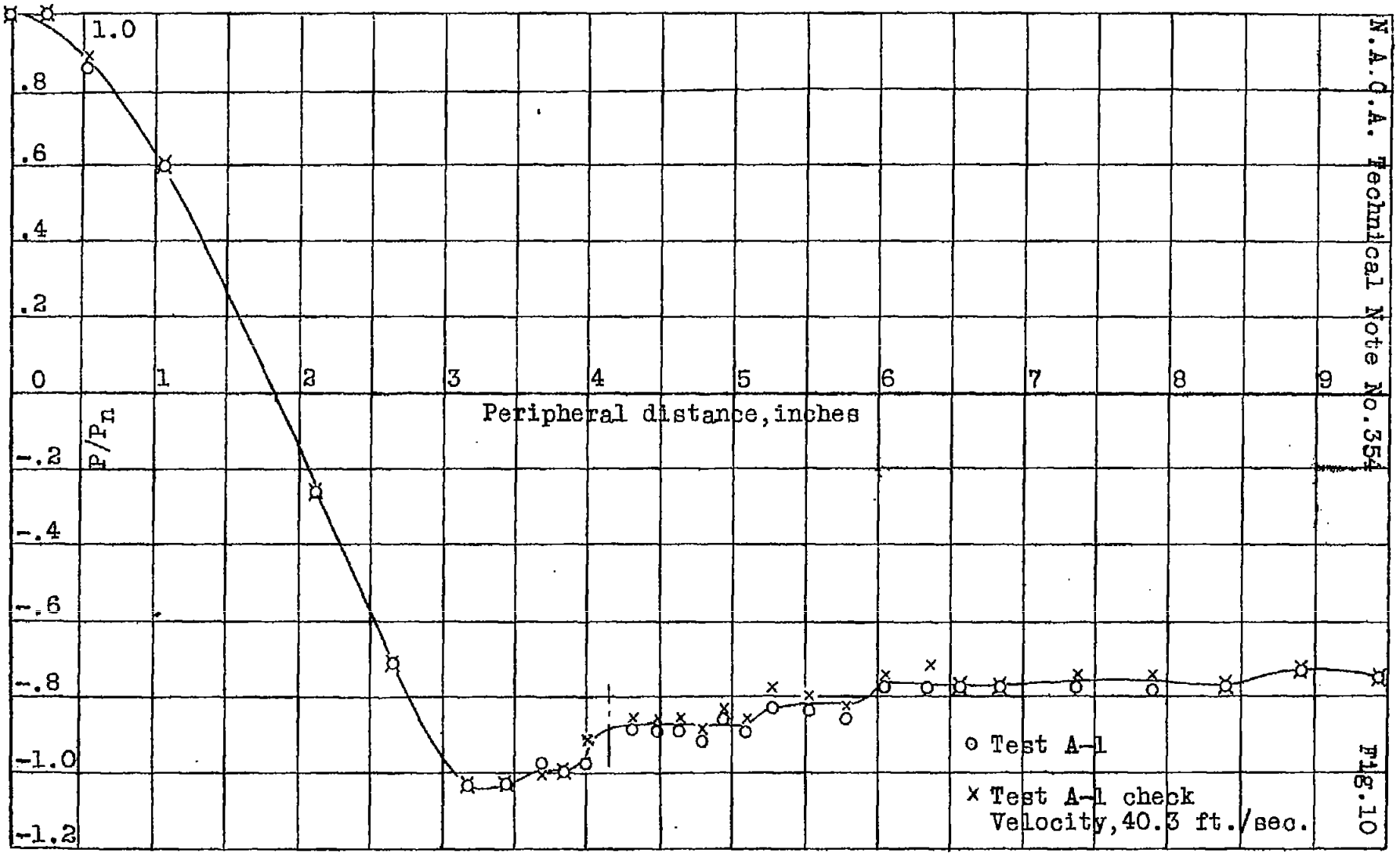

Fig.10 Pressure map, model A.

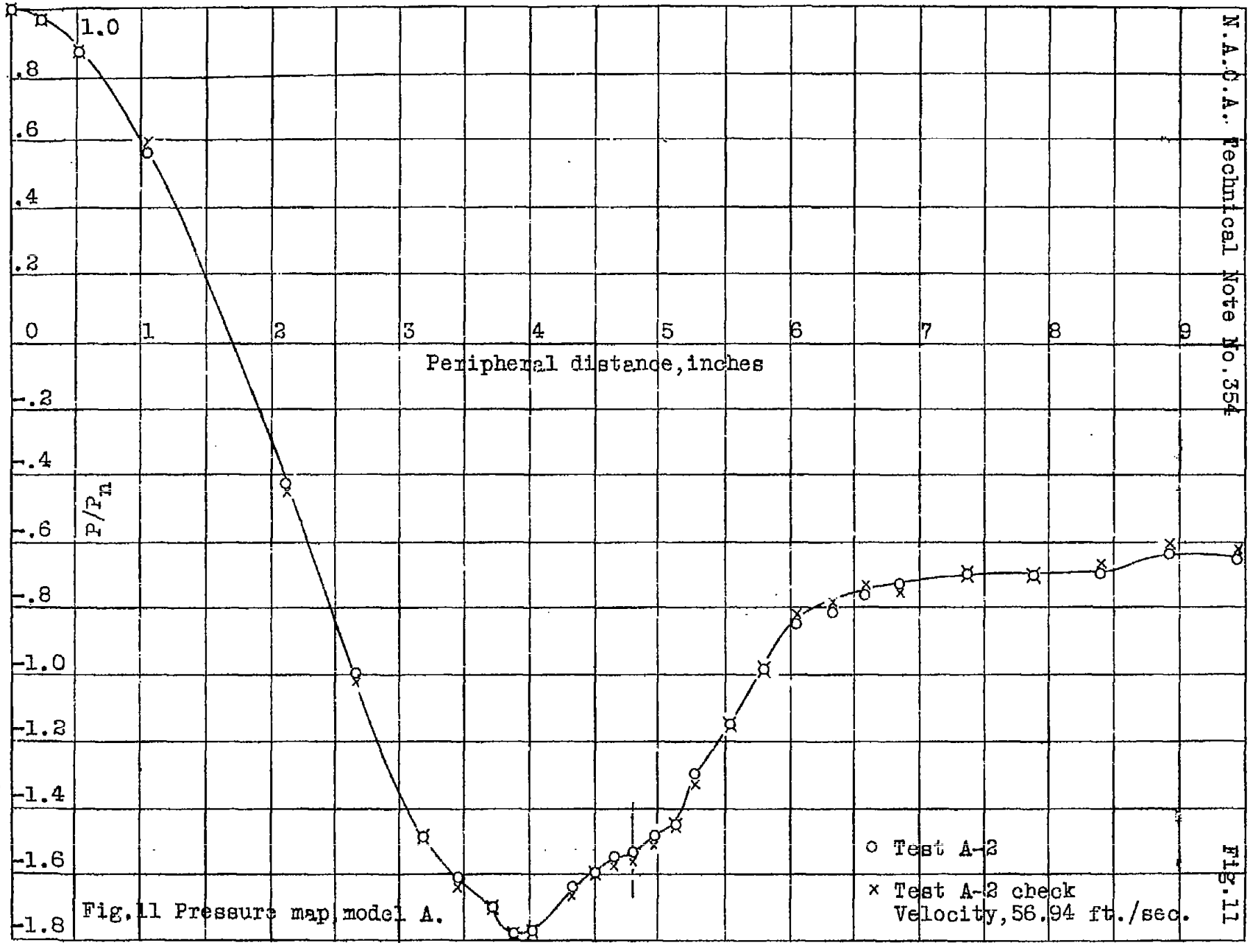

Fig.11 Pressure map, model A.

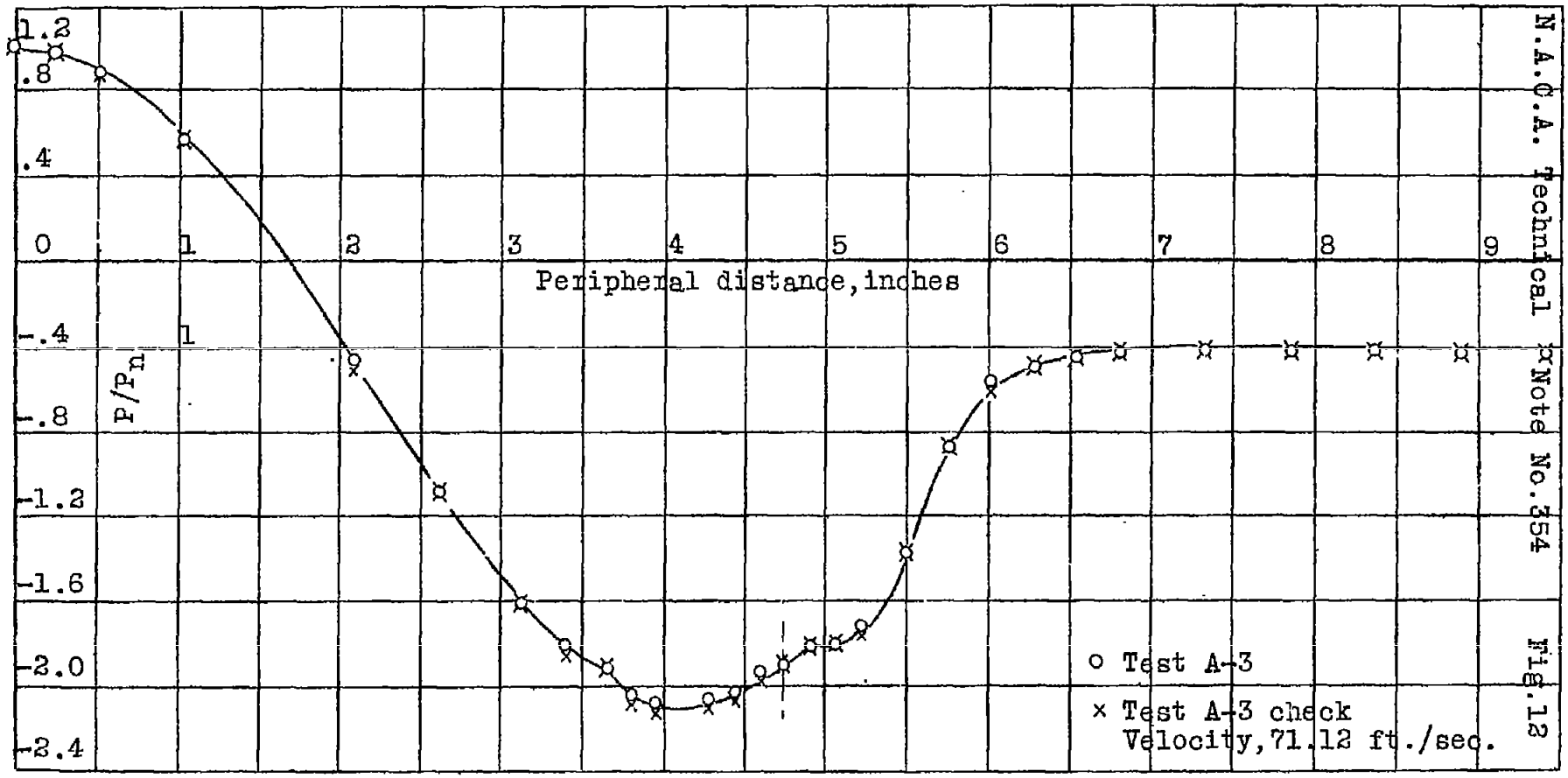

Fig.12 Pressure map, model A.

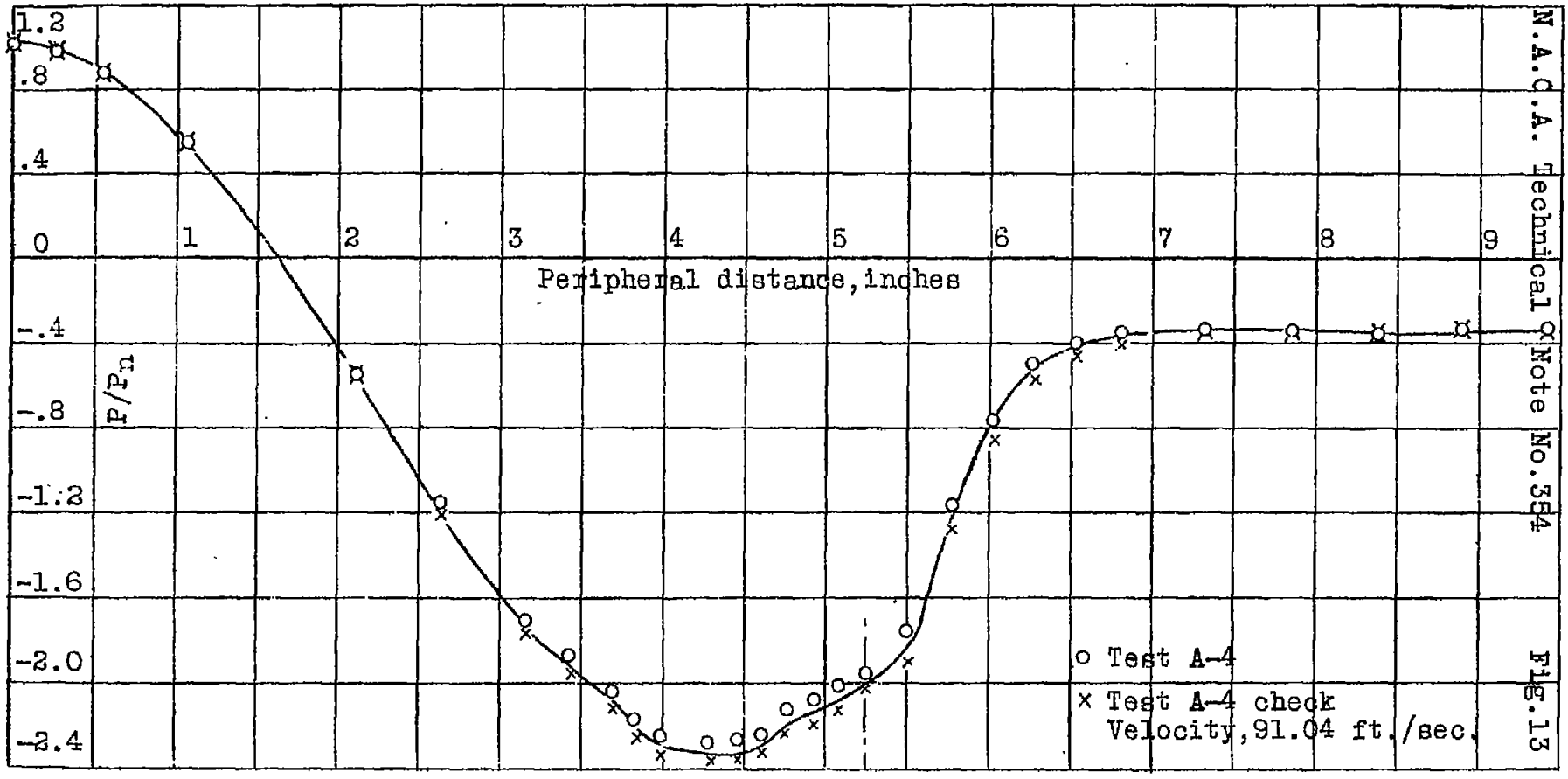

Fig.13 Pressure map, model A.

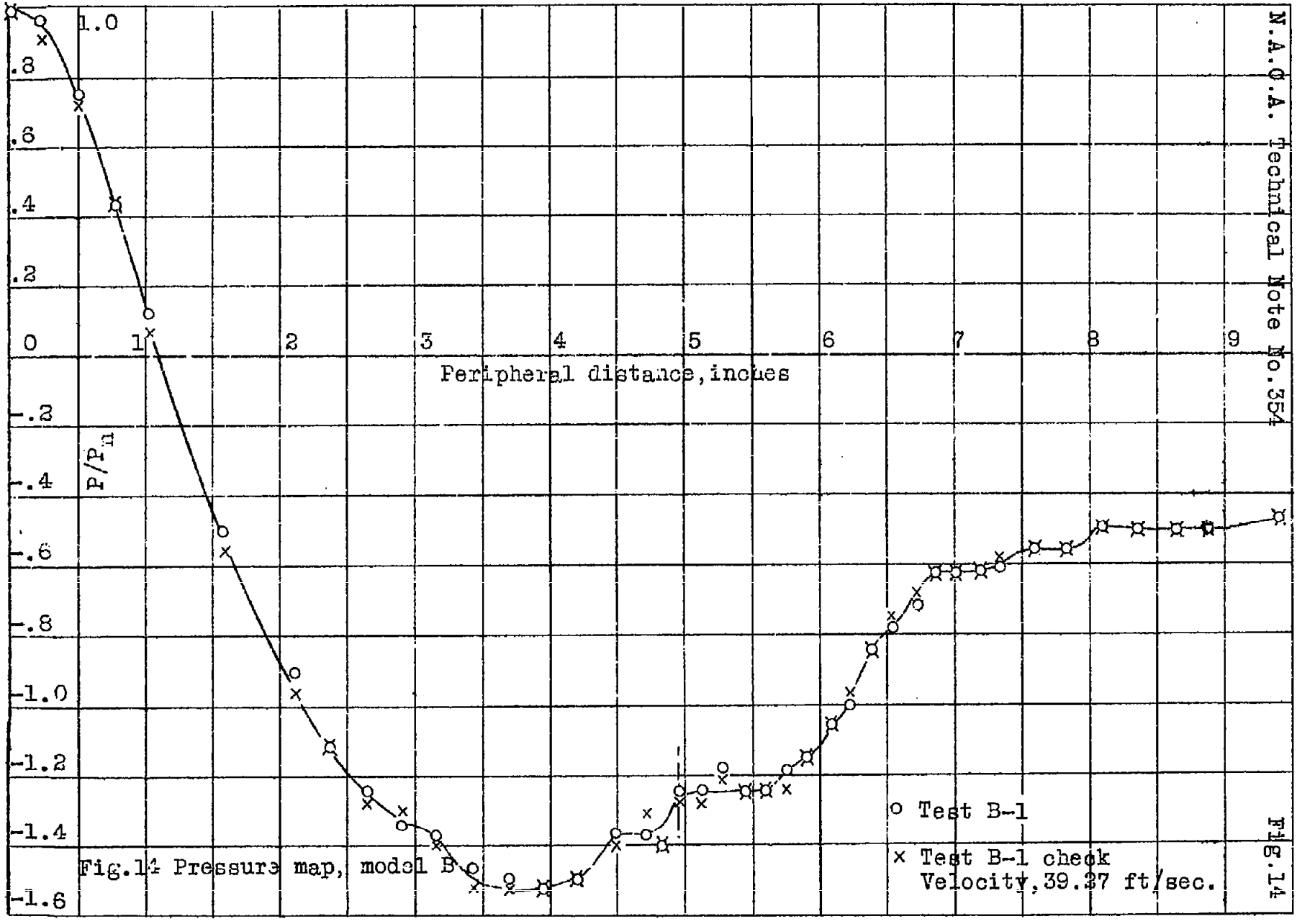

Fig.14 Pressure map, model B

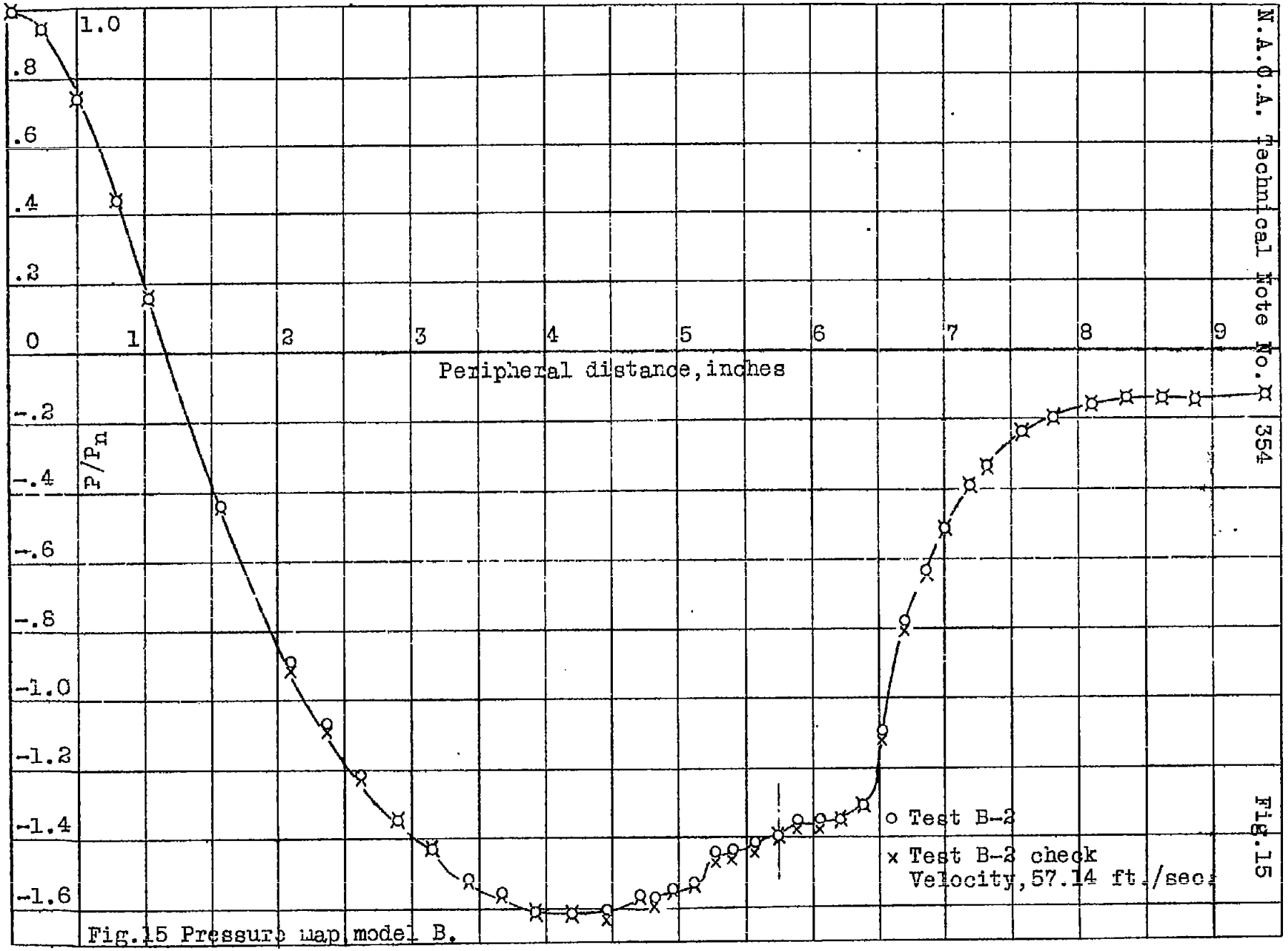

Fig.15 Pressure map model B.

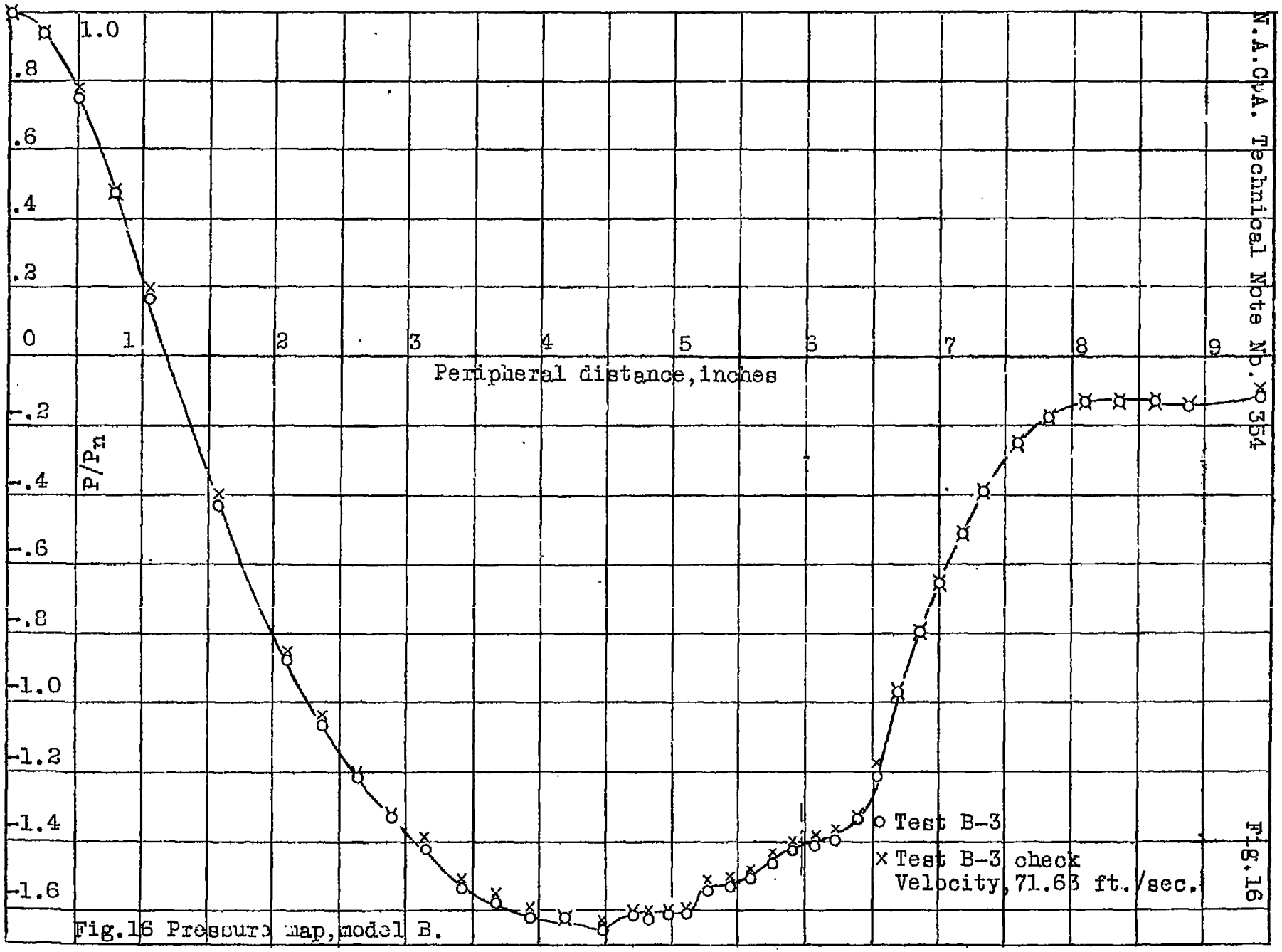

Fig.16 Pressure map, model B.

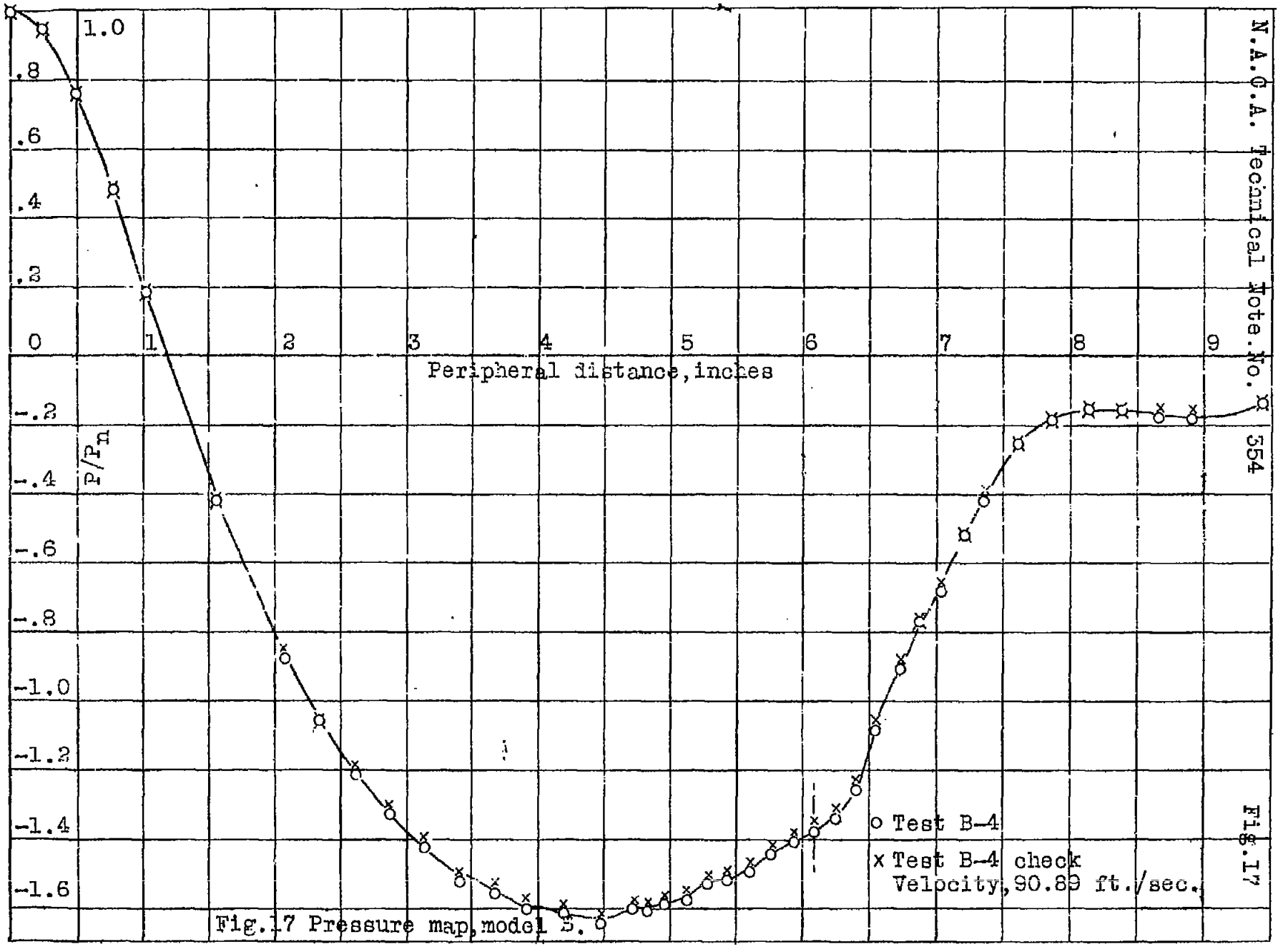

Fig.17 Pressure map, model B.

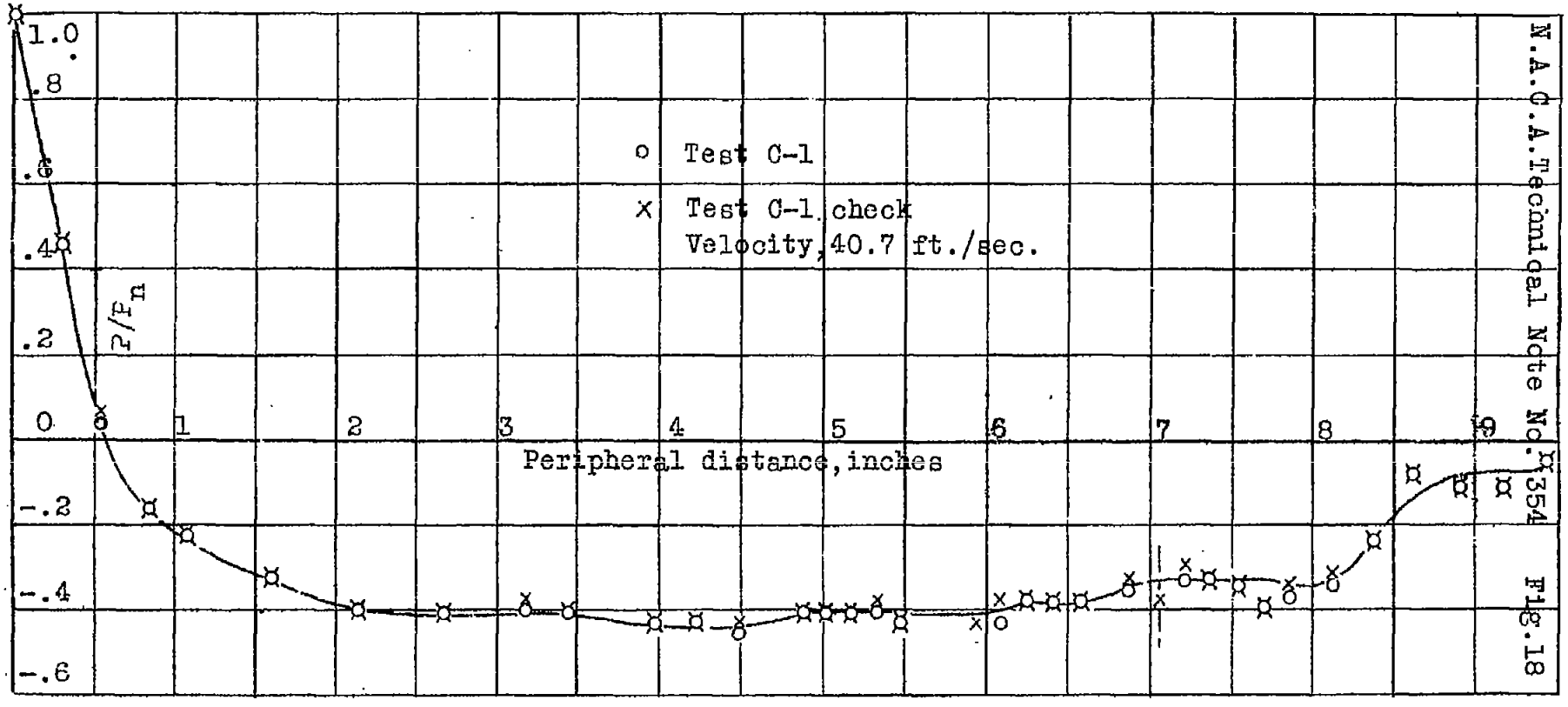

Fig.18 Pressure map, model C.

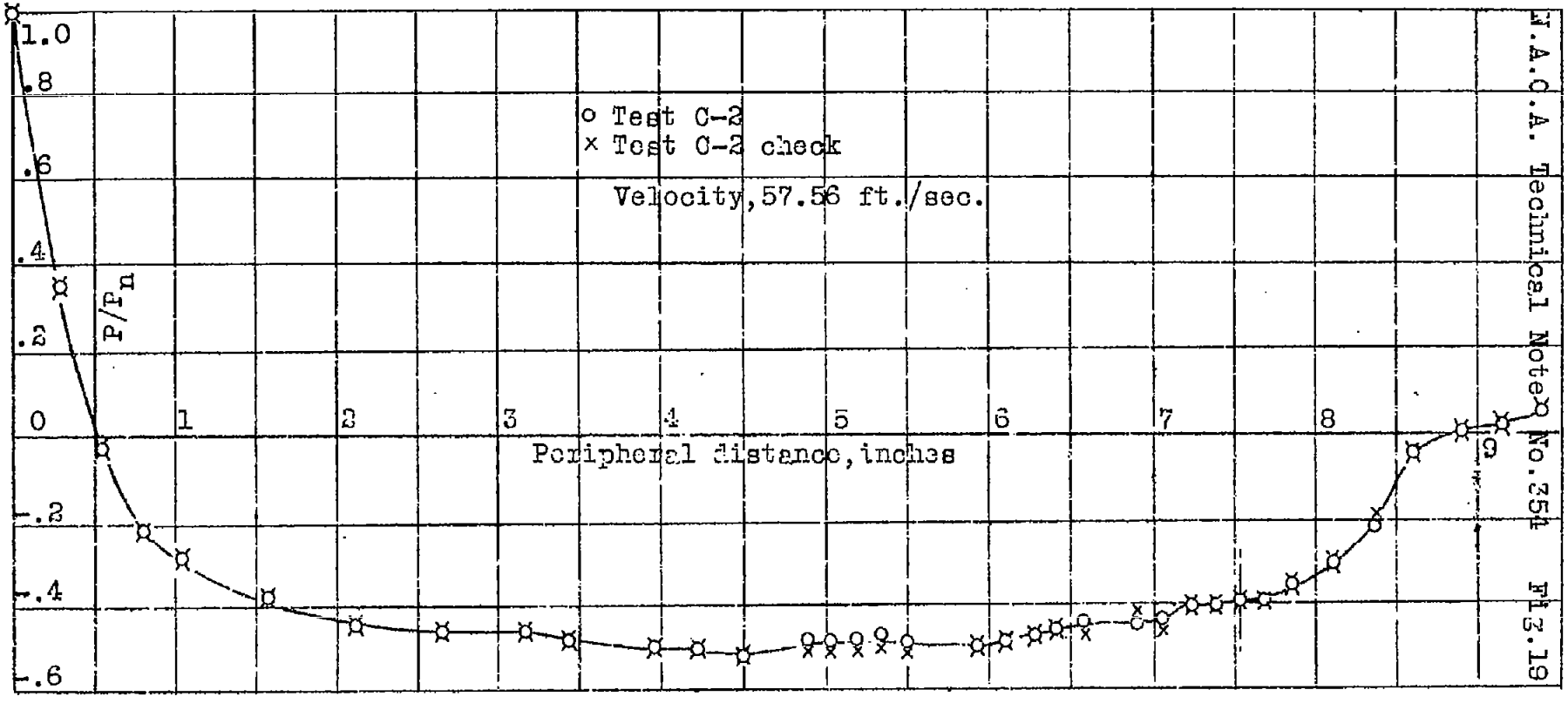

Fig.19 Pressure map, model C.

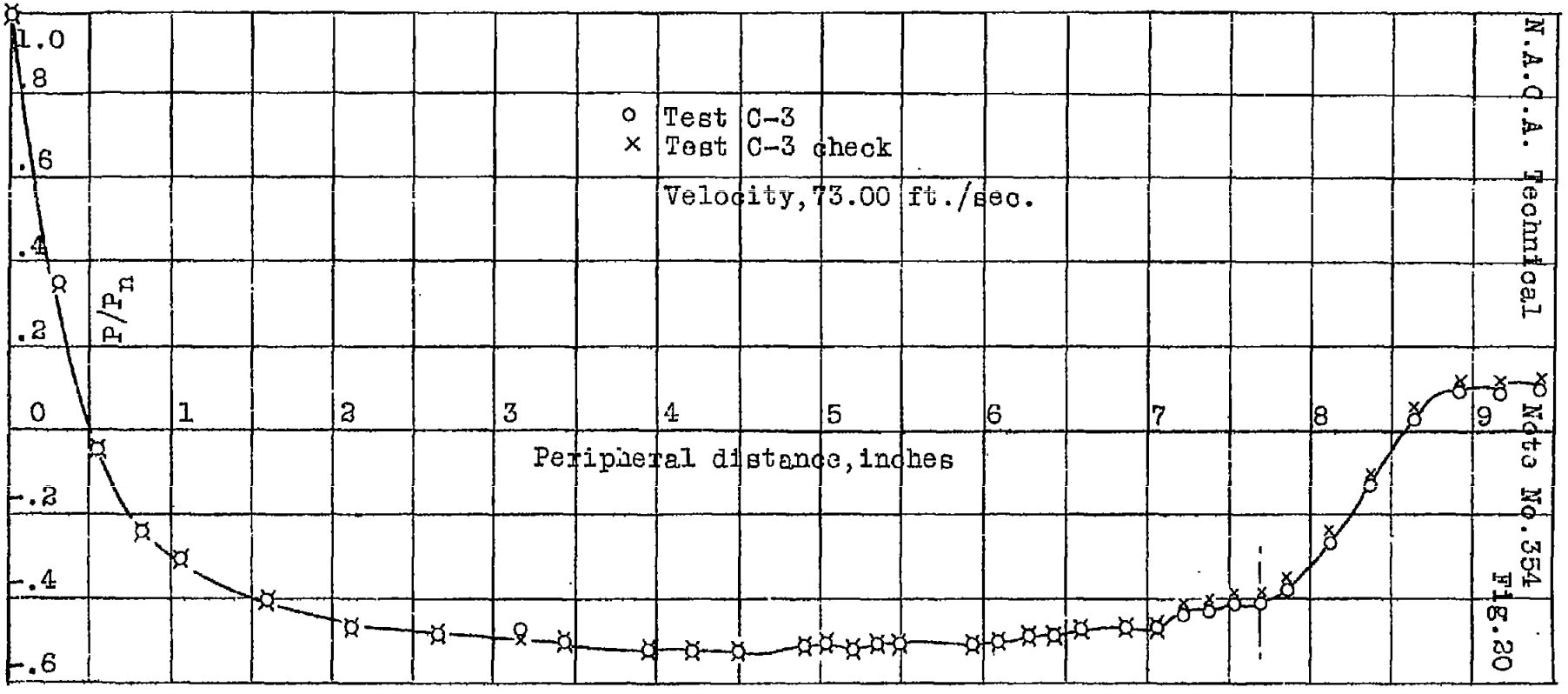

Fig.20 Pressure map, model C.

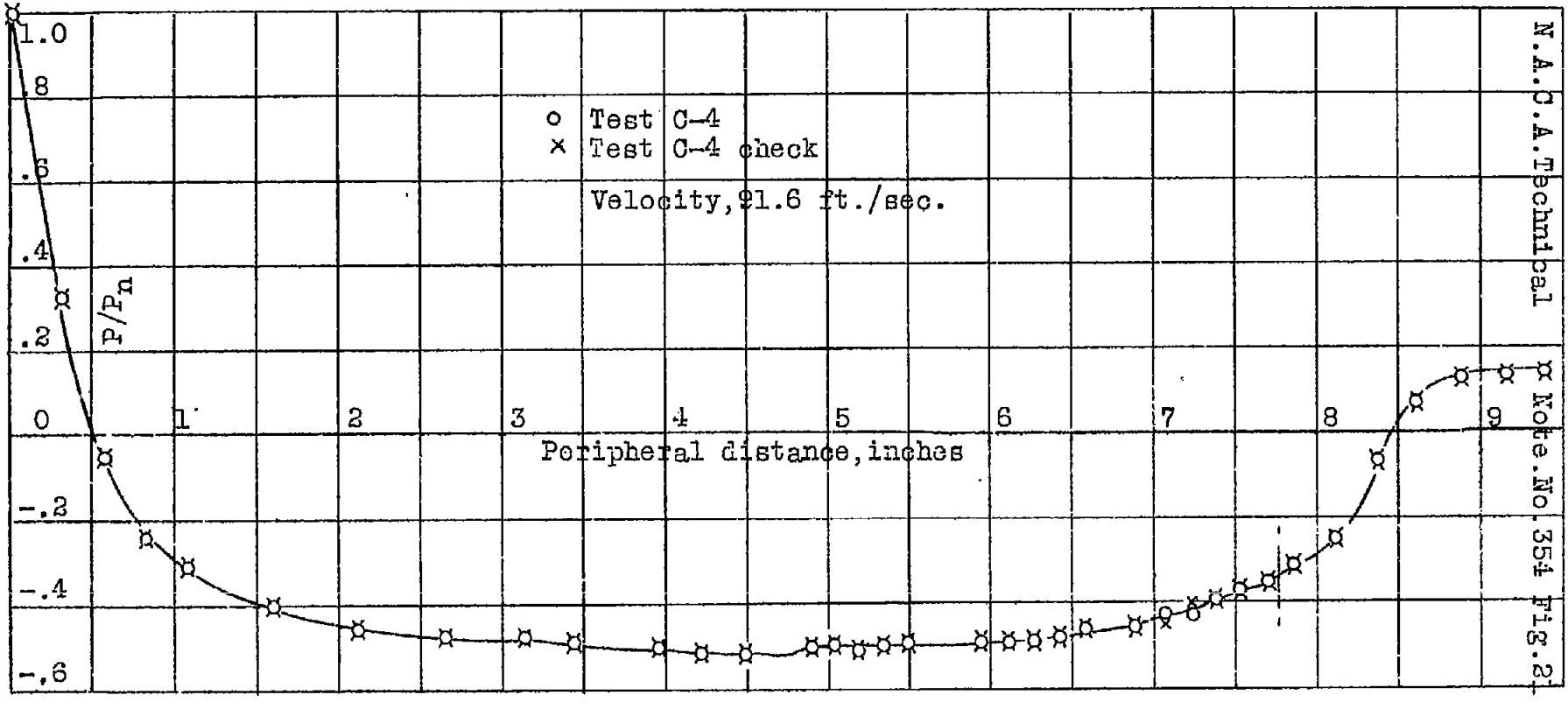

Fig.21 Pressure map, model C.

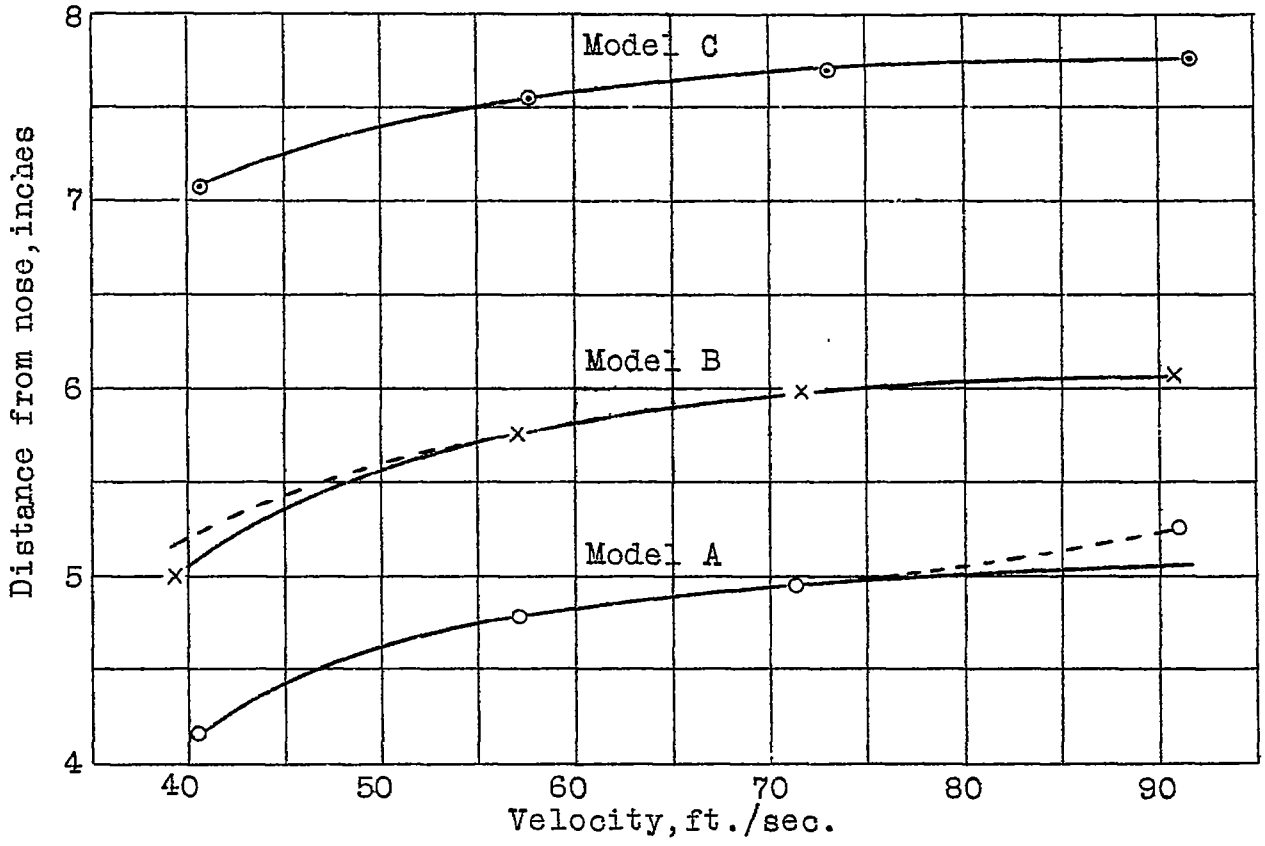

Fig.22 Recession of discontinuity with increase of velocity.

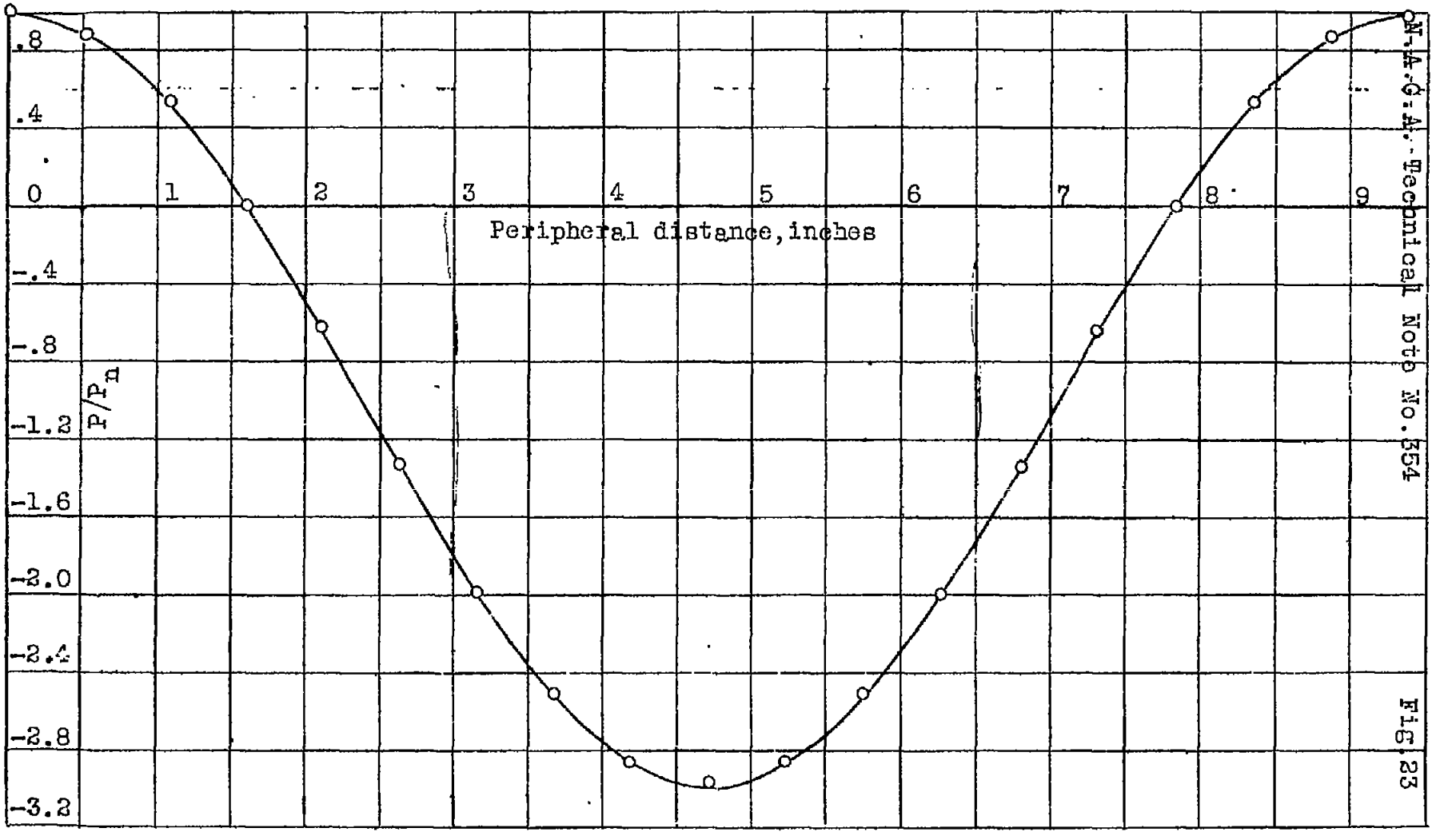

Fig.23 Theoretical pressure map, model A.

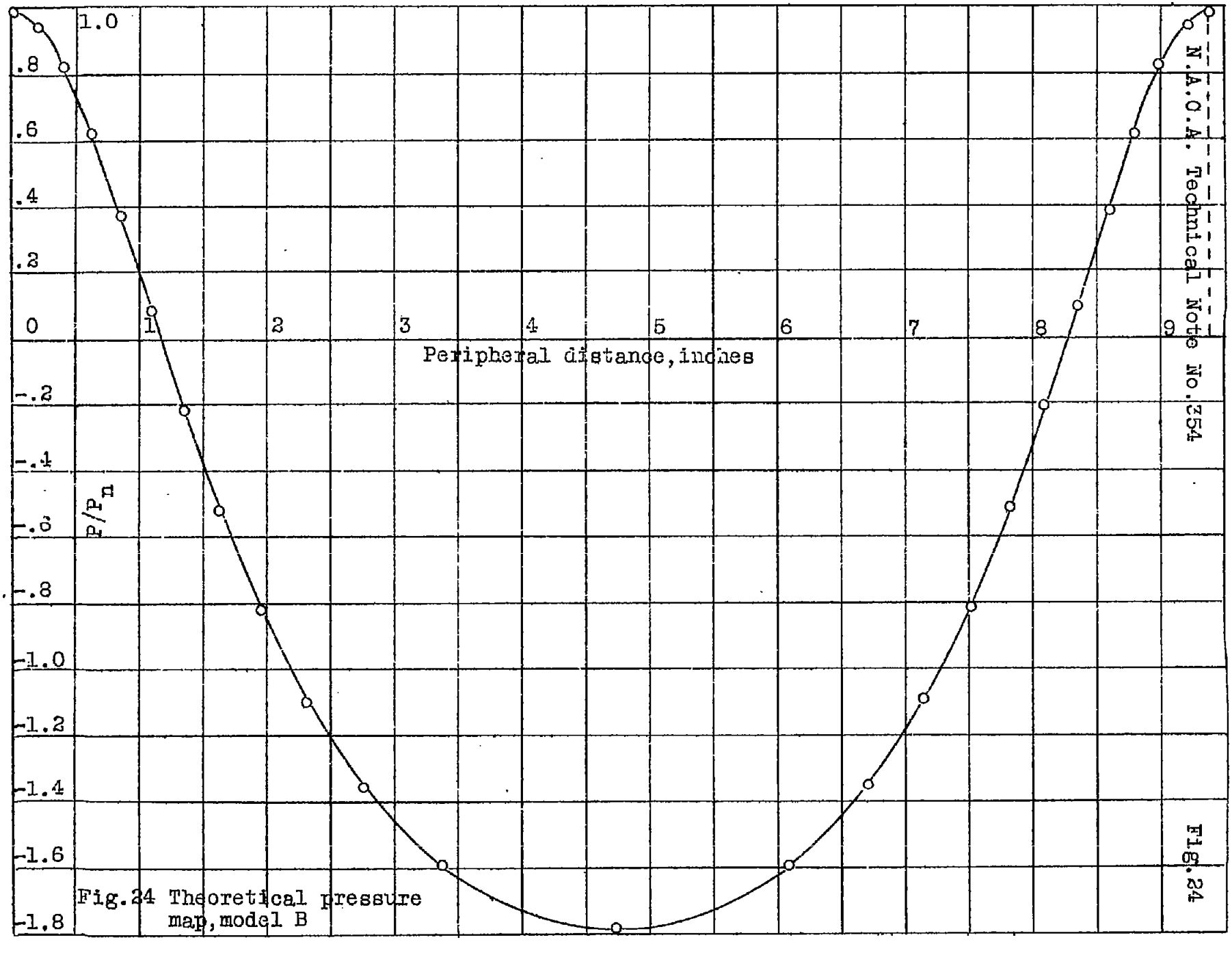

Fig.24 Theoretical pressure map, model B

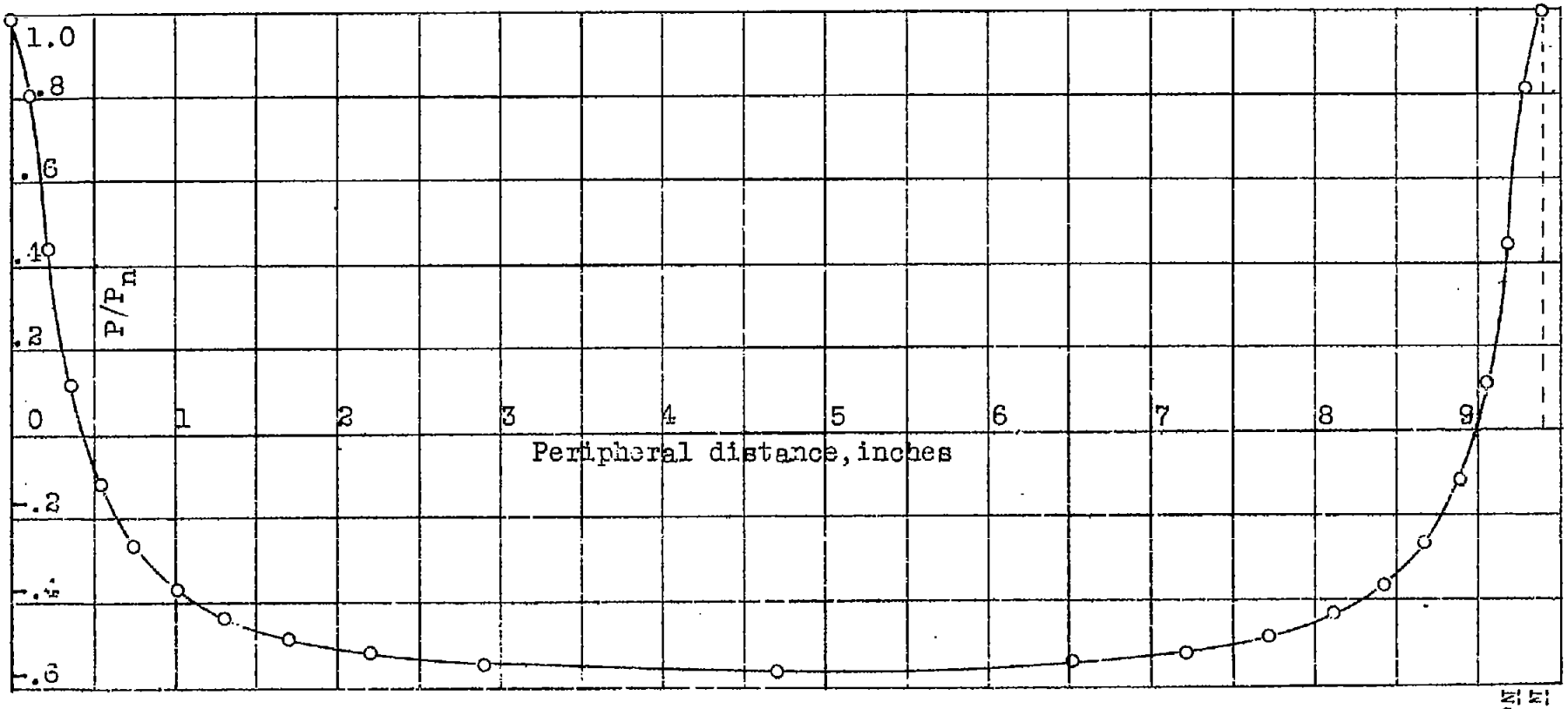

Fig.25 Theoretical pressure map, model C

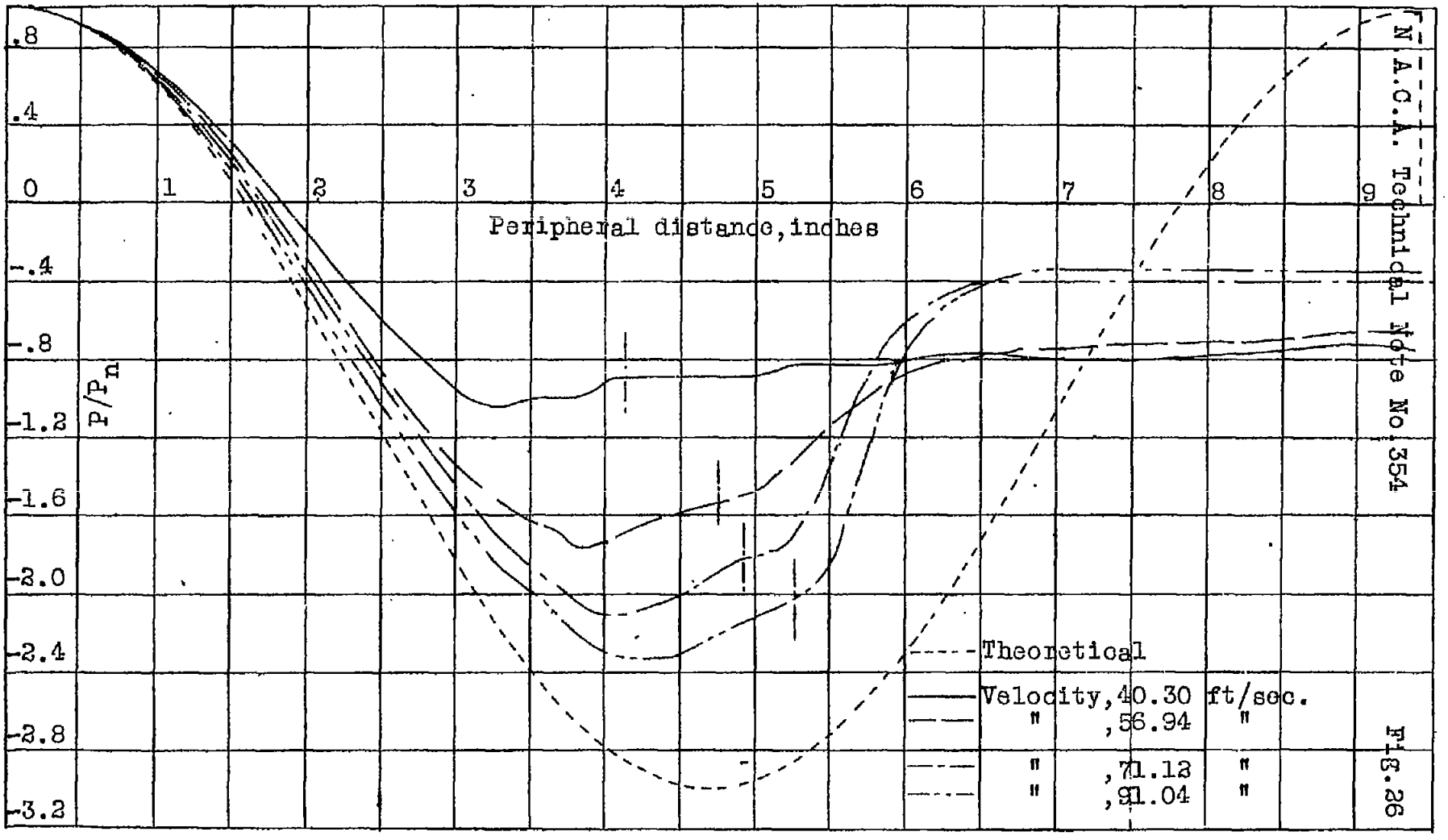

Fig. 26 Model A

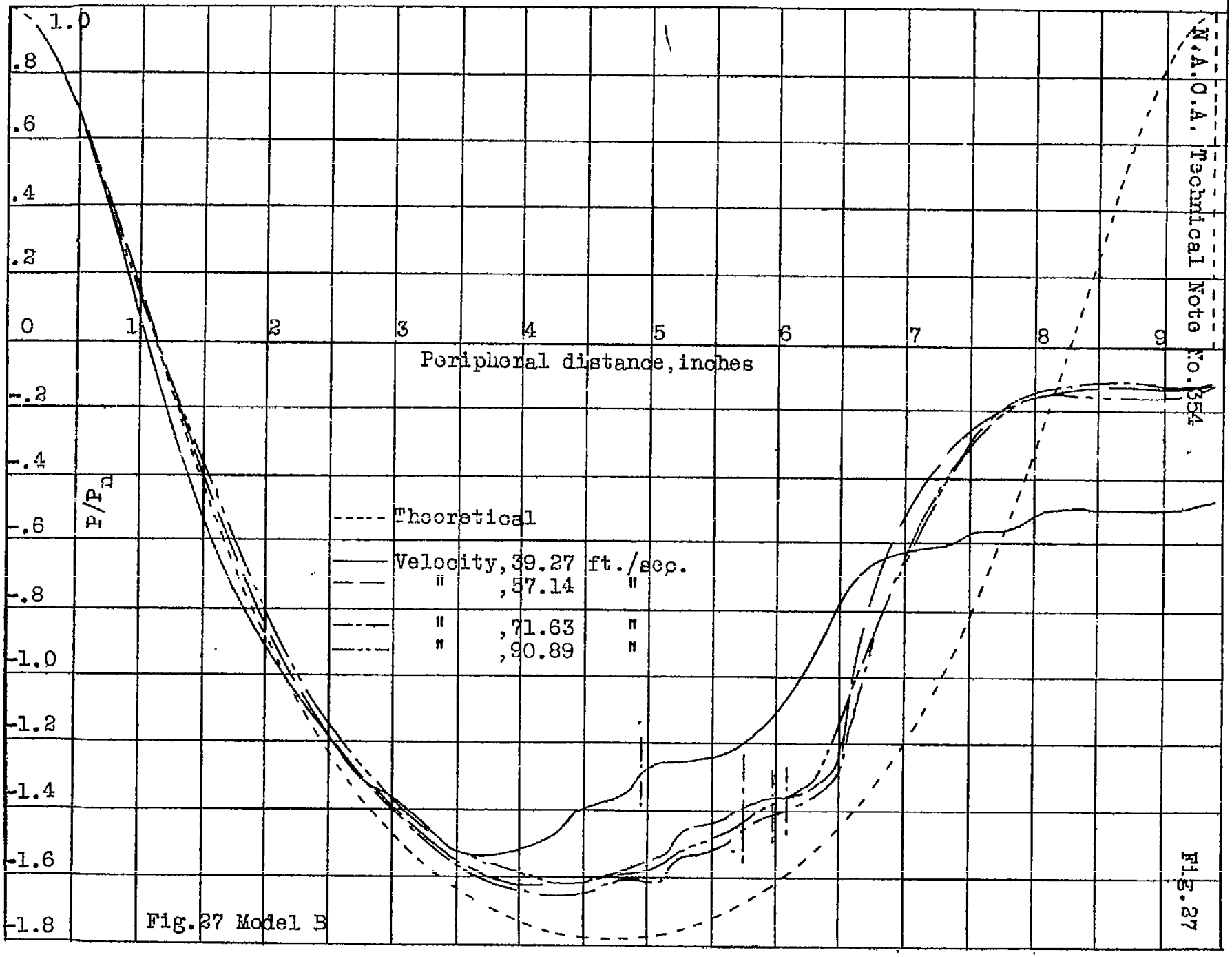

Fig. 27 Model B

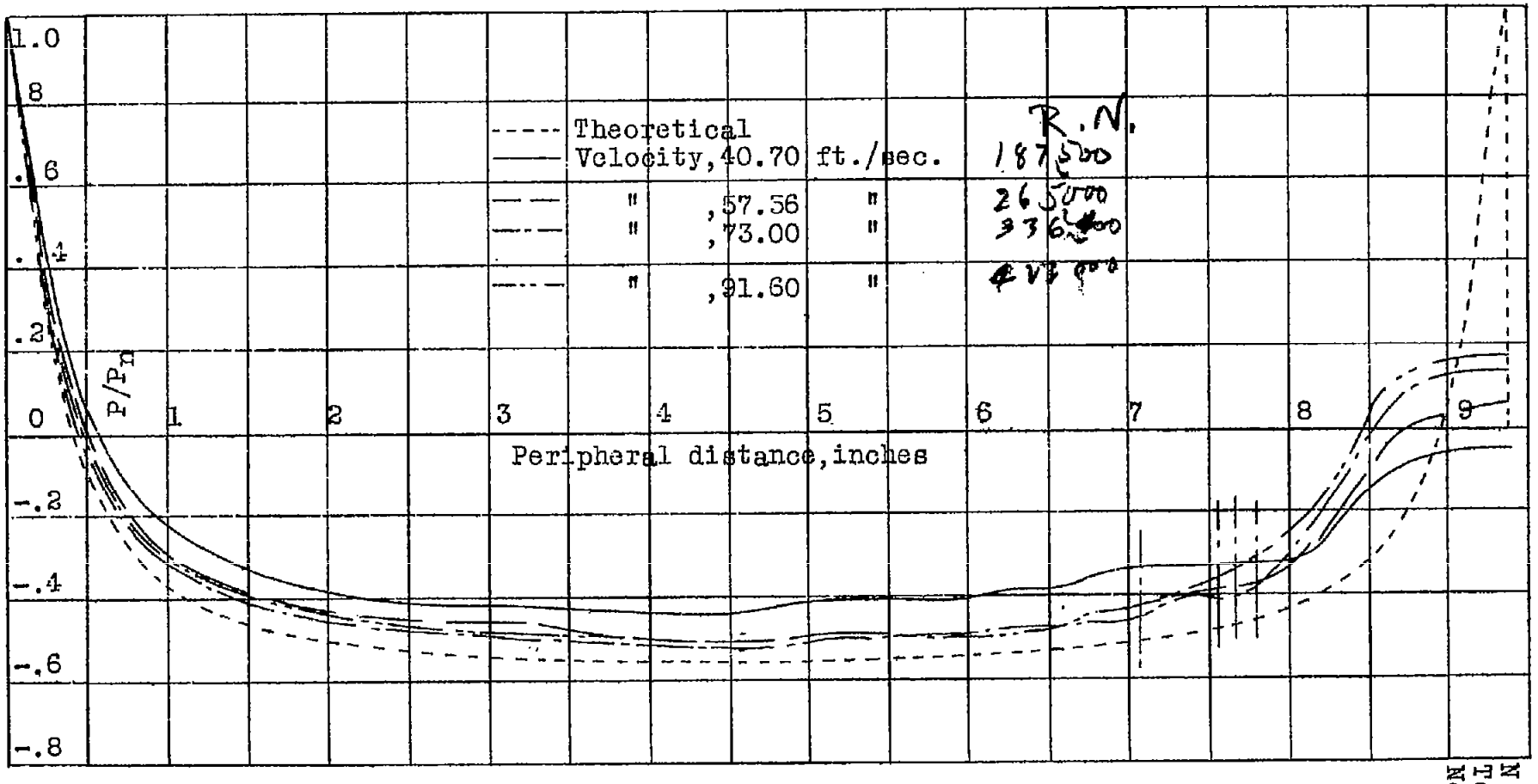

Fig.28 Model C